Reviews in Mineralogy & Geochemistry
Vol. 56, pp. 125-170, 2004

Spectroscopy of Epidote Minerals

Axel Liebscher

Department 4, Chemistry of the Earth
GeoForschungsZentrum Potsdam
Telegraphenberg
D 14473 Potsdam, Germany
alieb@gfz-potsdam.de

INTRODUCTION

Numerous spectroscopic techniques have been applied to the epidote minerals to characterize their structure and crystal chemistry. The substitution of transition metal ions Mn, Cr, and V, besides Fe, in the different crystallographic sites of epidote minerals and with different valence states has been studied by optical absorption spectroscopy. These studies mainly focused on the determination of (i) the site preferences of the different transition metal ions within the epidote minerals (e.g., Burns and Strens 1967; Tsang and Ghose 1971), (ii) the physical and structural characteristics of these sites as a function of composition, temperature and/or pressure (e.g., Taran and Langer 2000; Langer et al. 2002), (iii) their crystal field stabilization energy (e.g., Burns and Strens 1967; Langer et al. 2002), and (iv) the cause of the color and pleochroism in some epidote minerals (e.g., Faye and Nickel 1971). Major topics of infrared spectroscopic studies have been the proton environment and its changes with composition, temperature, and pressure (e.g., Langer and Raith 1974; Winkler et al. 1989; Della Ventura et al. 1996; Liebscher et al. 2002) and the phase transition within the orthorhombic solid solution series (e.g., Liebscher and Gottschalk 2004). Mössbauer spectroscopy has been used (i) to resolve the valence state of Fe in the different epidote minerals and its site location (e.g., Dollase 1973; Kartashov et al. 2002) and (ii) to study the intracrystalline Al-Fe partitioning between the different octahedral sites and the kinetic of this ordering process (e.g., Patrier et al. 1991; Fehr and Heuss-Aßbichler 1997).

This chapter reviews the different spectroscopic studies and techniques applied to epidote minerals with emphasis given to the crystal chemical results. An in-depth presentation and discussion of the different spectroscopic techniques and their theoretical framework is beyond the scope of this chapter. Additional information about spectroscopic studies of piemontite and allanite can be found in Bonazzi and Menchetti (2004) and Gieré and Sorensen (2004), respectively.

ULTRAVIOLET, VISIBLE AND NEAR-INFRARED SPECTROSCOPY

Most spectroscopic studies in the ultraviolet (UV), visible (VIS), and near-infrared (NIR) spectral range focused on the monoclinic epidote minerals. After the first spectral measurements of an Al-Fe^{3+} solid solution of unspecified composition reported by Grum-Grzhimailo et al. (1963), White and Keester (1966) published the 300 K spectrum below 25,000 cm^{-1} of a natural epidote with 17 wt% Fe_2O_3 and Marfunin et al. (1967) the spectra of epidote of unspecified composition. The first systematic spectroscopic study between

1529-6466/04/0056-0003$05.00

25,000 and 4,540 cm^{-1} stems from Burns and Strens (1967) who recorded the polarized absorption spectra of several natural Al-Fe-Mn-Cr epidotes of variable composition. Wood and Strens (1972) then used the piemontite spectra of Burns and Strens (1967) to test their method for calculating the crystal field splitting in distorted coordination polyhedra. Abu-Eid (1974) recorded the powder spectra of a natural piemontite at 10^{-4} and 19.7 GPa and Langer et al. (1976) and Langer and Abu-Eid (1977) reported the first polarized room temperature absorption spectra of synthetic piemontite single crystals. The first temperature dependent polarized absorption spectra between 23,000 and 7,000 cm^{-1} were published by Parkin and Burns (1980) at 293 to 573 K for an epidote with 15.8 wt% Fe_2O_3. Smith et al. (1982) recorded the polarized absorption spectra at room and liquid nitrogen (100 ± 10 K) temperature of a natural piemontite. Kersten et al. (1988) and Langer et al. (2002) performed further detailed spectroscopic studies on natural and synthetic piemontite samples. Taran and Langer (2000) recorded polarized absorption spectra, slightly extending the temperature range studied by Parkin and Burns (1980) to 600 K, and were the first to publish pressure dependent absorption spectra up to 9.6 GPa for an epidote with $X_{Ep} \sim 0.78$ [$X_{Ep} = Fe^{3+}/(\Sigma M^{3+} - 2)$].

So far, spectroscopic studies of the orthorhombic epidote minerals in the UV, VIS, and NIR spectral range are rare. Faye and Nickel (1971) studied the room temperature (polarized and unpolarized) absorption spectra of a tan (untreated and heat treated) and a blue colored natural V bearing zoisite. Schmetzer and Berdesinski (1978) recorded the absorption and remission spectra of natural Al-Fe^{3+} and of natural Cr^{3+} and V^{3+} bearing zoisite and Schmetzer and Bank (1979) studied the effect of heat treatment on the pleochroism of V^{3+} and V^{3+}-Cr^{3+} bearing zoisite. The polarized room temperature absorption spectra of natural and synthetic Mn^{3+} bearing zoisite were then reported by Petrusenko et al. (1992) and Langer et al. (2002).

The different studies cited display the recorded spectra either in the form of absorbance, linear absorption coefficient α, or molar extinction coefficient ε as a function of the wavelength or the wavenumber. To allow for easier comparison between the different studies, the wavelength values are generally converted to the corresponding wavenumbers throughout this review. Because the wavenumber is the reciprocal of the wavelength, the reader should be aware that the converted wavenumber scale of those spectra displayed in the figures that were originally presented as a function of wavelength is not linear. The other values, i.e., absorbance, linear absorption coefficient α, or molar extinction coefficient ε are not converted into a common unit as not all studies provide the necessary values (i.e., sample thickness, concentration). Likewise, the different studies use different terminologies to describe the respective polarization schemes. To be consistent, the terms X-, Y-, and Z-spectrum or X-, Y-, and Z-polarization are used throughout and designate polarization schemes in which the electrical vector **E** is parallel to one of the principal vibration directions **X**, **Y**, or **Z** of the indicatrix.

Optical absorption spectra of the monoclinic epidote minerals

Spectra of Al-Fe^{3+} solid solutions. Investigations of Al-Fe^{3+} solid solutions are restricted to the studies of Grum-Grzhimailo et al. (1963), White and Keester (1966), Burns and Strens (1967), Parkin and Burns (1980), Petrusenko et al. (1992), and Taran and Langer (2000). The reported spectra closely resemble each other. Although in the case of polarized spectra each polarization is distinctive, the spectra are generally characterized by weak bands in the VIS and NIR region and bands in the violet that are situated on the shoulder of the UV absorption edge. Typical polarized spectra of Fe^{3+} in epidote are shown in Figure 1a,b together with pressure dependent spectra (Fig. 1c) recorded with unpolarized light. All three polarizations are characterized by two bands at ~22,000 (band d) and ~21,200 (band c) cm^{-1}, with intensities in the order Z > Y > X (Fig. 1a,b). In addition, the X-spectrum contains a weak inflection at ~17,900 cm^{-1} (band b) and a weak band at ~12,000 cm^{-1} (band a), the Y-spectrum two pronounced inflections at ~17,900 cm^{-1} (band b) and 11,100 cm^{-1} (band a), and the Z-spectrum

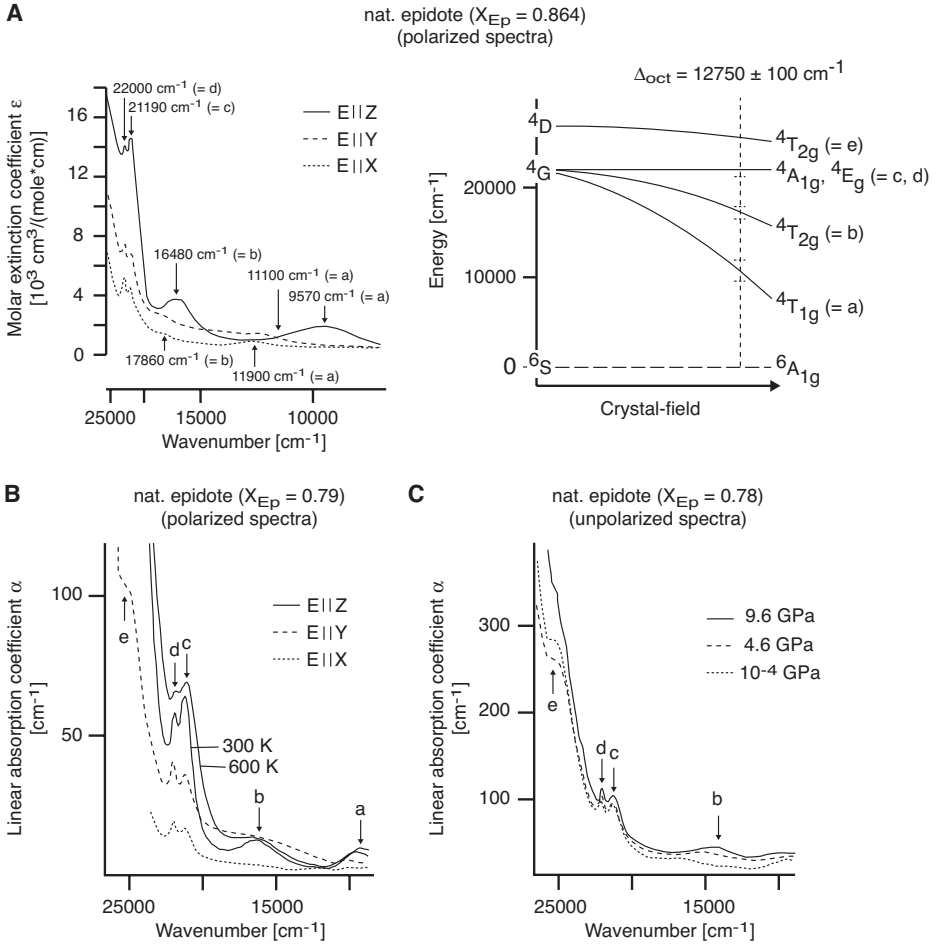

Figure 1. (A) Polarized room-temperature absorption spectra of a natural epidote with X_{Ep} = 0.864. The spectra show four bands a to d that arise from spin forbidden *dd* transitions. The simplified energy level diagram shows only those spin forbidden *dd* transitions that are relevant for the observed absorption bands. (B) Polarized absorption spectra of a natural epidote with X_{Ep} = 0.79 at 300 and 600 K. For clarity only the Z-spectrum is shown for 600 K. In addition to the bands a to d, the Y-spectrum at 300 K displays a shoulder on the UV absorption edge (band e). (C) Unpolarized absorption spectra of a natural epidote with X_{Ep} = 0.78 at 10^{-4}, 4.6, and 9.6 GPa. The position of the bands c, d, and e is independent on pressure whereas the band b shows a notable pressure shift to lower wavenumber. Redrawn and modified after Burns and Strens (1967) and Taran and Langer (2000).

two well-defined bands at ~16,500 cm^{-1} (band b) and 9,600 cm^{-1} (band a) (Fig. 1a,b). In the Y-spectrum a fifth band at ~25,100 cm^{-1} (band e) occurs as a prominent shoulder on the absorption edge (Fig. 1b,c; Taran and Langer 2000).

The Fe^{3+} ion has a d^5 electronic configuration and thus only spin forbidden *dd* transitions occur. The observed bands below 25,000 cm^{-1} in the spectra of Fe^{3+} in epidote are generally assigned to the spin forbidden *dd* transitions ${}^6A_{1g} \rightarrow {}^4T_{1g}$ (${}^4G$) (band a), ${}^6A_{1g} \rightarrow {}^4T_{2g}$ (${}^4G$) (band b), ${}^6A_{1g} \rightarrow {}^4E_g$ (${}^4G$) (band c), and ${}^6A_{1g} \rightarrow {}^4A_{1g}$ (${}^4G$) (band d) (Fig. 1a; Burns and Strens 1967;

Taran and Langer 2000). The band e at about 25,100 cm^{-1} observed in the Y-spectrum by Taran and Langer (2000; Fig. 1b,c) may arise from the spin forbidden *dd* transition $^6A_{1g} \rightarrow {}^4T_{2g}$ (^4D) (see Fig. 1a; Taran and Langer 2000). The absorption edge is due to $O^{2-} \rightarrow Fe^{3+}$ charge-transfer transitions (Petrusenko et al. 1992; Taran and Langer 2000). From the position of the observed bands shown in Figure 1a, Burns and Strens (1967) calculated the crystal field splitting parameter Δ_{oct} to 12,750 ± 100 cm^{-1} for the investigated epidote with $X_{Ep} = 0.864$.

Bruns and Strens (1967) studied the compositional dependence of the spectral properties of Fe^{3+} in monoclinic Al-Fe^{3+} solid solutions within the range $X_{Ep} = 0.155$ to 0.915. At low Fe contents the weak inflections in the Y- and X-spectra become inconspicuous and only the weak to well-defined bands in the X- and Z-spectra are still apparent. With increasing Fe content the absorption maxima of bands a and b in the Z-spectra move to lower wavenumber whereas the absorption maximum of band a in the X-spectra moves to higher wavenumber. The two bands c and d are not resolved in the spectra of low Fe epidote but appear as only one band at ~22,200 cm^{-1}, which is asymmetric on the low wavenumber side. With increasing Fe content the bands c and d become resolved and their absorption maxima are shifted to lower wavenumber. Over the compositional range $X_{Ep} = 0.155$ to 0.915 Δ_{oct} varies from 13,200 ± 100 to 12,700 ± 100 cm^{-1} (Burns and Strens 1967).

The influence of temperature on the spectral properties of Fe^{3+} in epidote has been studied by Parkin and Burns (1980) up to 573 K and by Taran and Langer (2000) up to 600 K. With increasing temperature, the intensity of the absorption edge strongly increases (Fig. 1b; Taran and Langer 2000). The data of Taran and Langer (2000) indicate that (i) the absorption maxima of bands a and b shift with about 0.85 cm^{-1} K^{-1} upon heating, (ii) the half-width of both bands broadens with increasing temperature although with a different temperature dependence (band a: 0.03 cm^{-1} K^{-1}, band b: 0.74 cm^{-1} K^{-1}), and (iii) the integral intensities of both bands slightly shift with temperature in an opposite sense (band a: -1×10^{-5} K^{-1}, band b: 8×10^{-4} K^{-1}) (Fig. 1b). These results are partly in contradiction to the findings of Parkin and Burns (1980) for a temperature increase from 293 to 473 K, who found (i) a shift of the absorption maximum of band a (Z-spectrum) to lower wavenumber of ~700 cm^{-1} (i.e., −3.9 cm^{-1} K^{-1}), (ii) a constant position for the absorption maximum of band b (Z-spectrum), (iii) constant half-widths of bands a and b, and (iv) a slight intensity increase for band a. The spectra recorded by Taran and Langer (2000) further show that band c shifts with −0.4 cm^{-1} K^{-1} to lower wavenumber on heating whereas the position of band d remains practically unchanged resulting in a slight increase of the splitting between bands c and d (Fig. 1b). The half-width of the bands c and d broadens with 0.6 cm^{-1} K^{-1} and 0.8 cm^{-1} K^{-1}, respectively, and their integral intensities decrease with -2.2×10^{-4} K^{-1} and -0.9×10^{-4} K^{-1}, respectively, with raising temperature (Taran and Langer 2000). These findings for bands c and d are in agreement with the results of Parkin and Burns (1980) although the latter also found a slight shift of band d to lower wavenumber upon heating.

Taran and Langer (2000) recorded the unpolarized absorption spectra of an epidote with X_{Ep} ~0.78 at 10^{-4}, 4.6, and 9.6 GPa (Fig. 1c). In these spectra the bands b, c, d, and e appear as well defined absorption maxima. In the spectrum taken at 10^{-4} GPa the positions of these bands closely resemble those of the corresponding bands in the polarized spectra (compare Fig. 1b). With increasing pressure, only the absorption maximum of band b significantly shifts with −242 cm^{-1} GPa^{-1} to lower wavenumber and its half-width decreases with −32.3 cm^{-1} GPa^{-1} (Fig. 1c; Taran and Langer 2000). Neither band c nor band d show any change in position or half-width with increasing pressure (Fig. 1c; Taran and Langer 2000). The integral intensities of all bands remain almost constant (Taran and Langer 2000). Up to about 5 GPa the intensity of the absorption edge slightly decreases followed by a strong increase upon further pressure increase. At 9.6 GPa the shoulder that it caused by band e and that is clearly seen at lower pressure is almost hidden by the absorption edge (Fig. 1c).

Based on the observed temperature dependence of the absorption bands, Taran and Langer (2000) concluded that the M3 octahedron retains its distortion or gets only slightly more distorted with increasing temperature. From the temperature shift of band a they calculated the local thermal expansion coefficient α_{loc} for the M3 octahedron to about 0.9×10^{-5} K^{-1}. The lack of a pressure shift of the position of bands c and d confirms that the covalent bonding of Fe^{3+}–O in the M3 octahedron does not change significantly with pressure (Taran and Langer 2000). From the pronounced pressure shift of band b Taran and Langer (2000) obtained a compression modulus K_{poly} for the Fe^{3+} bearing M3 octahedron of about 75 GPa, which implies a comparable high compressibility of M3 within the epidote structure.

Spectra of natural and synthetic piemontite. After Burns and Strens (1967) had recorded the first polarized VIS and NIR absorption spectra of six natural piemontite samples, Abu-Eid (1974) published the powder spectra of a natural piemontite of unspecified composition at 10^{-4} and 19.7 GPa. Later, Langer et al. (1976) recorded the first polarized absorption spectra of a synthetic piemontite. Smith et al. (1982) then studied the polarized absorption spectra of a natural piemontite at room and liquid nitrogen temperature within the spectral range 30,000 to 10,000 cm^{-1} and Taran et al. (1984) those of natural Mn clinozoisites. Pressure dependent polarized spectra of a natural piemontite up to 7.7 GPa are reported by Langer (1990). Most recently, Langer et al. (2002) performed a detailed spectroscopic study in the spectral range 35,000 to 5,000 cm^{-1} on several natural and synthetic piemontite samples.

All reported spectra of Mn^{3+} in natural as well as synthetic piemontite closely resemble each other in their principal spectral properties (Figs 2a, 3). They are dominated by a slightly polarized UV absorption edge. Within the VIS and NIR spectral range, the spectra are characterized by three intense and strongly polarized absorption bands ν_I, ν_{II}, and ν_{III} (Figs 2, 3, 5). Band ν_I is centered between 13,000 and 12,000 cm^{-1} and is strongly polarized with intensities in the order Y-spectrum >> Z- and X-spectrum. Band ν_{II} has its maximum absorption between 19,000 and 18,000 cm^{-1} and can be identified in all three polarizations

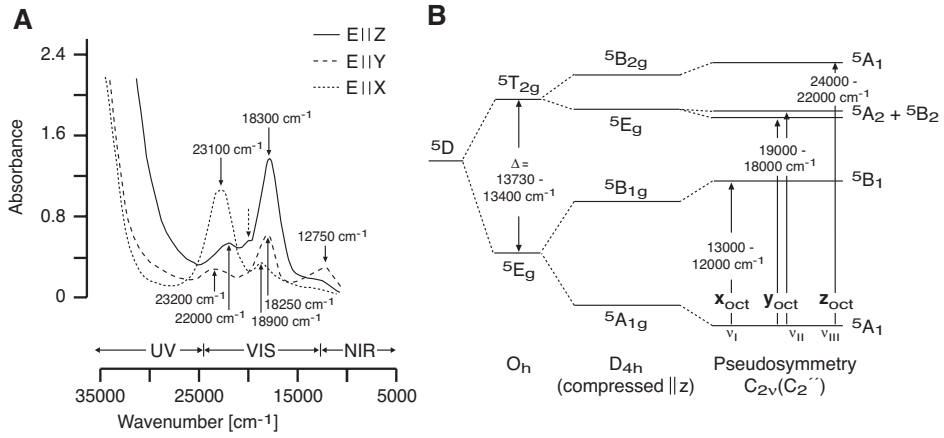

Figure 2. (A) Polarized room-temperature absorption spectra of synthetic piemontite between 35,000 and 10,000 cm^{-1}. Solid arrows denote bands ν_I, ν_{II}, and ν_{III} that can be assigned to spin allowed *dd* transitions of Mn^{3+}. The stippled arrow at ~20,000 cm^{-1} denotes a band that probably arises from a spin forbidden *dd* transition of Mn^{3+}. (B) Energy level diagram for the proposed pseudosymmetry $C_{2v}(C_2^{''})$ showing the spin allowed *dd* transitions responsible for the bands ν_I, ν_{II}, and ν_{III}. $\mathbf{x}_{oct}$, $\mathbf{y}_{oct}$, and $\mathbf{z}_{oct}$ denote the polarization of the bands ν_I, ν_{II}, and ν_{III} with respect to the internal axes of the M3 octahedron. For the relation of the internal axes to the principal axes of the indicatrix see text. Redrawn and modified after Langer et al. (1976) and Langer et al. (2002).

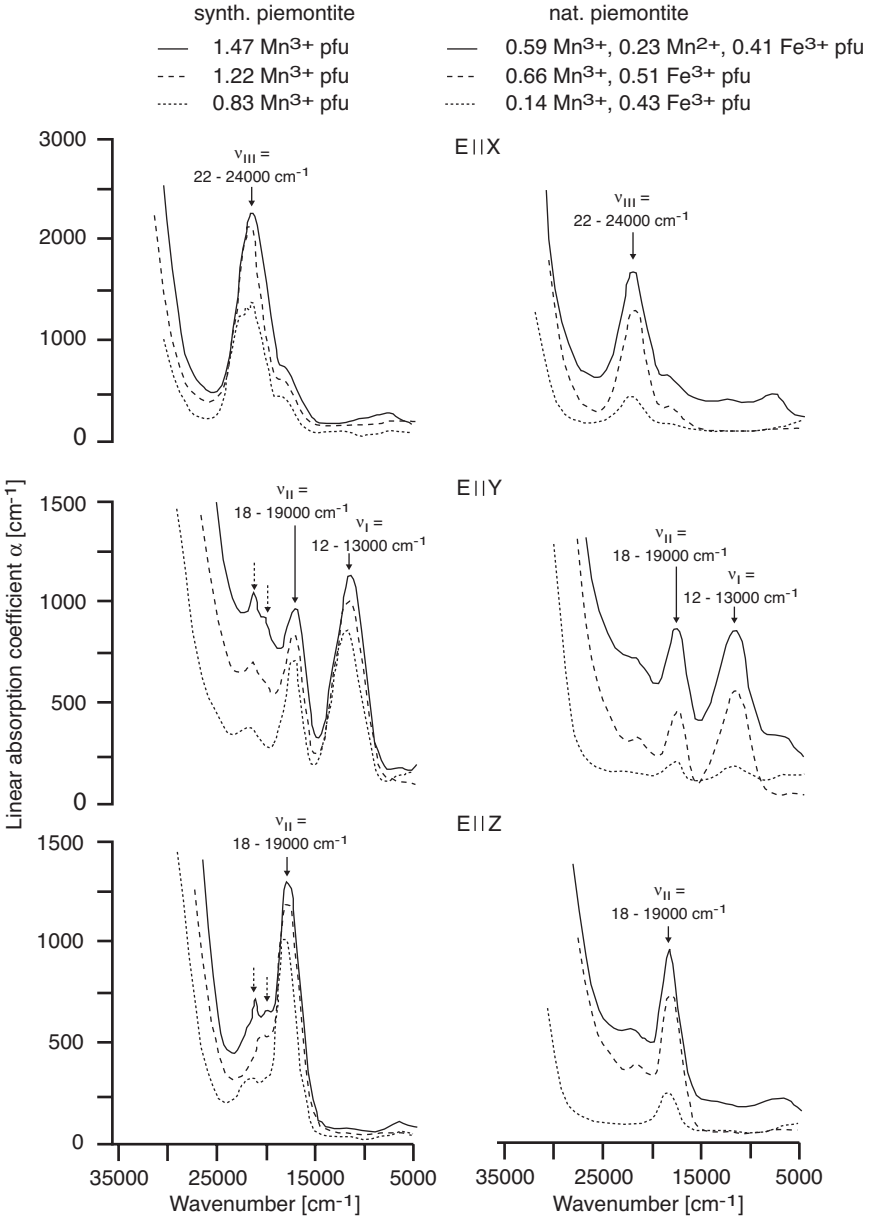

Figure 3. Polarized room temperature absorption spectra of synthetic (left) and natural (right) piemontite. Solid arrows denote the bands ν_I, ν_{II}, and ν_{III} that arise from the spin allowed *dd* transitions of Mn^{3+} in M3. Stippled arrows denote bands that either arise from spin forbidden *dd* transitions of Mn^{3+} in M3 or from spin allowed *dd* transitions of Mn^{3+} in M1. Redrawn and modified after Langer et al. (2002).

with intensities Z-spectrum >> Y-spectrum > X-spectrum. The third band ν_{III} appears between 24,000 and 22,000 cm^{-1} and has strong polarization with intensities in the order X-spectrum >> Y- and Z-spectrum. The strong polarization of the main bands ν_I, ν_{II}, and ν_{III} accounts for the trichroic scheme in piemontite with **X** = yellow, **Y** = violet red, and **Z** = carmine (Langer et al. 2002). In addition to these main bands, the Y- and Z-spectra of some synthetic and natural piemontite samples display weak but distinct bands or shoulders in the spectral range 22,000 to 20,000 cm^{-1} in (Figs 2,3; Langer et al. 1976; Langer and Abu-Eid 1977; Smith et al. 1982; Petrusenko et al. 1992; Langer et al. 2002).

The strong and almost complete polarization of the bands ν_I, ν_{II}, and ν_{III} cannot be explained on the basis of the site symmetry C_s of the M3 octahedron (Langer et al. 2002) and the authors postulate the pseudosymmetry $C_{2v}(C_2'')$ for M3. The derived energy level diagram for the pseudosymmetry $C_{2v}(C_2'')$ is well in accord with the number of the observed bands and their polarizations (Fig. 2b) as the orientation of the internal octahedral axes $\mathbf{x}_{oct}$, $\mathbf{y}_{oct}$, and $\mathbf{z}_{oct}$ shown in Figure 2b relative to the optical indicatrix axes is $\mathbf{x}_{oct} = \mathbf{Y}$, $\mathbf{y}_{oct} \sim \mathbf{Z}$, and $\mathbf{z}_{oct} \sim \mathbf{X}$ (Langer et al. 2002). Based on the energy level diagram for the pseudosymmetry $C_{2v}(C_2'')$, Langer et al. (2002) assigned the bands ν_I, ν_{II}, and ν_{III} to the spin allowed *dd* transitions $^5A_1 \rightarrow {}^5B_1$ (^5D) (band ν_I), $^5A_1 \rightarrow {}^5A_2 + {}^5B_2$ (^5D) (band ν_{II}), and $^5A_1 \rightarrow {}^5A_1$ (^5D) (band ν_{III}) (Fig. 2b). The weak but distinct bands between ~22,000 and 20,000 cm^{-1} can be assigned to either spin allowed *dd* transitions of Mn^{3+} in the M1 octahedron or to spin forbidden *dd* transitions of Mn^{3+} in M3 (Langer et al. 2002). As M1 is centrosymmetric, the intensity of the bands that arise from the spin allowed *dd* transitions of Mn^{3+} in M1 will be significantly lower (at least one order of magnitude) than the intensity of the bands that arise from the spin allowed *dd* transitions of Mn^{3+} in M3 and will be partly or fully superimposed by the latter (Burns and Strens 1967; Langer et al. 2002).

The influence of composition on the spectral properties of Mn^{3+} in piemontite has been studied by Burns and Strens (1967) and Langer et al. (2002) for natural piemontite and by Langer et al. (2002) also for synthetic piemontite. With increasing Mn^{3+} content the UV absorption edge shifts to lower wavenumber (Figs 3, 4b). This shift is most pronounced in the Y-spectra (Fig. 4b). Within the VIS and NIR spectral range the intensity and thus the linear absorption coefficient α of the bands ν_I, ν_{II}, and ν_{III} generally increase with increasing Mn^{3+} substitution (Fig. 3, 4a) and the absorption maxima of the bands ν_I, ν_{II}, and ν_{III} slightly shift to lower wavenumber (Fig. 4a). The crystal field splitting Δ_{oct} (calculated as $\Delta_{oct} = \nu_{III} - 2(\nu_{III} - \nu_{II})/3 - \nu_I/2$; Langer et al. 2002) decreases with increasing Mn^{3+} substitution (Burns and Strens 1967; Langer et al. 2002). Consequently, the octahedral crystal field stabilization energy (CFSE) of Mn^{3+} in M3 (calculated as $CFSE_{Mn3+(M3)} = 6\Delta_{oct}/10 + \nu_I/2$; Langer et al. 2002) decreases slightly on increasing Mn^{3+} substitution in M3 by about 200 cm^{-1} or 2.4 kJ/g-atom per 0.1 Mn^{3+} (Fig. 4c; Langer et al. 2002).

Smith et al. (1982) recorded the polarized absorption spectra of a natural piemontite with 0.829 Mn^{3+} and 0.346 Fe^{3+} pfu (per formula unit) at room and liquid nitrogen temperature (Fig. 5). The spectra display the typical features of Mn^{3+} in M3 as outlined above: In the spectra recorded at liquid nitrogen temperature the bands ν_I, ν_{II}, and ν_{III} appear at 12,300 cm^{-1} (ν_I), 18,600 to 17,600 cm^{-1} (ν_{II}), and 22,000 to 21,600 cm^{-1} (ν_{III}) with their characteristic intensity ratios and polarizations. Beside these main bands, Smith et al. (1982) further observed a band at 15,600 cm^{-1} in the X- and Z-spectra, a fine structure of ν_{III} in the Y- and Z-spectra displaying shoulders at about 22,500 and 20,600 cm^{-1}, and two weak bands at 24,600 and 23,700 cm^{-1} in the liquid nitrogen Z-spectrum (Fig. 5). By comparing the recorded spectra with those reported by Burns and Strens (1967) for Fe^{3+} in epidote and by Langer et al. (1976) for synthetic piemontite, Smith et al. (1982) tentatively assigned these additional bands to the following spin forbidden *dd* transitions in Mn^{3+} and Fe^{3+}: (i) bands at 24,600 and 23,700 cm^{-1}: $^6A_{1g} \rightarrow {}^4T_{2g}$ (^4D) in Fe^{3+}, (ii) band at 22,500 cm^{-1}: $^6A_{1g} \rightarrow {}^4A_{1g}$, ^4E_g (^4G) in Fe^{3+}, band at ~20,600 cm^{-1}: $^5A_{1g} \rightarrow {}^3T_{1g}$ (^3H) in Mn^{3+}, and (iv) band at 15,600 cm^{-1}: $^6A_{1g} \rightarrow {}^4T_{2g}$ (^4G) in Fe^{3+}.

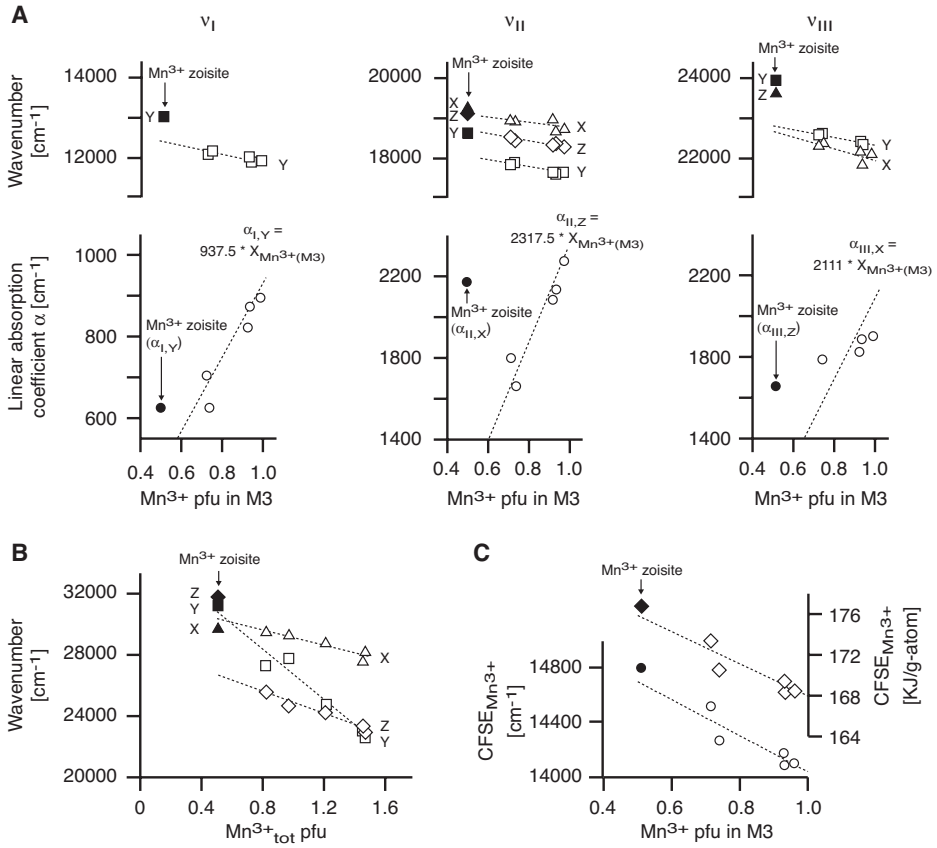

Figure 4. Compositional dependence of (A) position and linear absorption coefficient α for the bands ν_I, ν_{II}, and ν_{III}, (B) the position of the UV absorption edge, and (C) the crystal field stabilization energy $CFSE_{Mn3+(M3)}$ in synthetic piemontite (open symbols) and Mn^{3+} zoisite (closed symbols). X, Y, and Z denote the polarization. The linear absorption coefficient α is calculated for the polarization with maximum intensity for the respective band. The position of the absorption edge is defined as the wavenumber at which the linear absorption coefficient α is 1,200 cm^{-1} above the background. Note the different x-axis values: Mn^{3+} pfu in M3 in (A) and (C) and Mn^{3+}_{tot} pfu in (B). Stippled lines are linear fits to the piemontite data. Redrawn and modified after Langer et al. (2002).

The influence of pressure on the spectral properties of piemontite has so far only be studied for two natural piemontite samples by Abu-Eid (1974) and Langer (1990). Abu-Eid (1974) reports the powder spectra of a natural piemontite of unspecified composition at 10^{-4} and 19.7 GPa. On raising pressure the absorption maxima of the bands ν_I (12,000 → 12,250 cm^{-1}), ν_{II} (18,170 → 20,200 cm^{-1}), and ν_{III} (22,000 → 23,250 cm^{-1}) shift to higher wavenumber and the crystal field splitting Δ_{oct} increases from 13,450 to 15,092 cm^{-1} (Abu-Eid 1974). Assuming a linear behavior, these values correspond to pressure shifts of ~13 cm^{-1}/GPa (ν_I), ~103 cm^{-1}/GPa (ν_{II}), ~63 cm^{-1}/GPa (ν_{III}), and ~83 cm^{-1}/GPa (Δ_{oct}). From the pressure dependence of Δ_{oct}, Abu-Eid (1974) calculated a compression modulus K_{poly} for the Mn^{3+} bearing M3 octahedron of about 280 GPa. This compression modulus is rather high compared to the bulk modulus of piemontite, which Abu-Eid (1974) reports to 107 GPa, and the author therefore concludes, "the octahedral site is rather incompressible suggesting that the Ca-polyhedra take up most

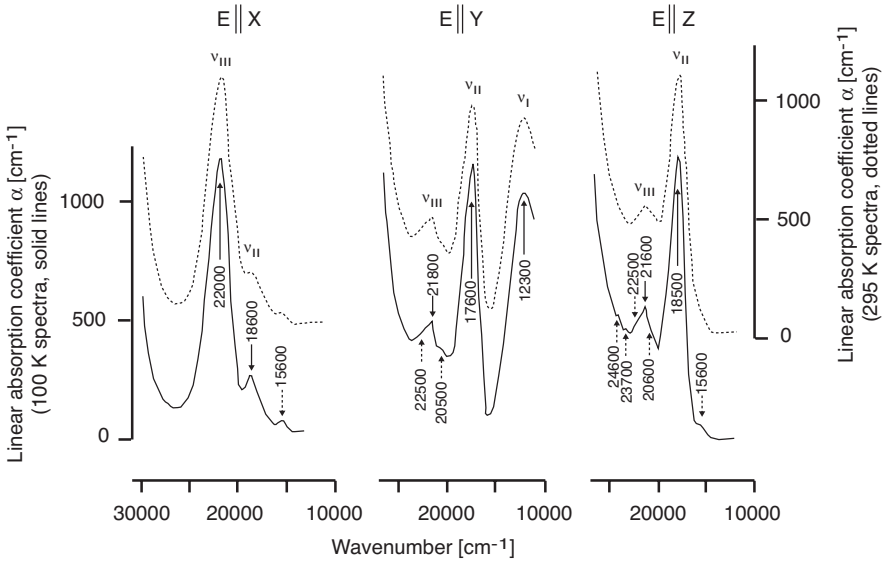

Figure 5. Polarized room temperature (stippled) and liquid-nitrogen (solid) spectra of natural piemontite. Solid arrows denote bands ν_I, ν_{II}, and ν_{III} arising from spin allowed *dd* transitions of Mn^{3+} in M3 whereas stippled arrows denote bands arising from spin forbidden *dd* transitions of Mn^{3+} (band at ~20,600 cm^{-1}) and Fe^{3+} (bands at ~24,600, 23,700, 22,500, and 15,600 cm^{-1}) in M3. Redrawn and modified after Smith et al. (1982).

of the change in volume." This high compression modulus and the conclusion of Abu-Eid (1974) are in sharp contrast to the results obtained by Taran and Langer (2000) for Fe^{3+} in M3 (see above). Unfortunately, with the data at hand this discrepancy cannot be resolved. Langer (1990) reports the Y-spectra of a natural piemontite of unspecified composition at 10^{-4}, 1.7, 3.7, and 7.7 GPa. Due to the experimental setup only the positions of the UV absorption edge and the bands ν_{II} and ν_{III} were recorded. With increasing pressure the UV absorption edge shifts to lower wavenumber whereas the absorption maxima of the bands ν_{II} (17,600 cm^{-1} at 10^{-4} GPa $\rightarrow$ 19,000 cm^{-1} at 7.7 GPa) and ν_{III} (21,800 cm^{-1} at 10^{-4} GPa $\rightarrow$ 22,500 cm^{-1} at 7.7 GPa) shift to higher wavenumber, consistent with the results of Abu-Eid (1974). The different pressure shift of the bands ν_{II} (=182 cm^{-1}/GPa) and ν_{III} (= 91 cm^{-1}/GPa) leads to a decrease of the energy difference between ν_{III} and ν_{II} with increasing pressure. The observed pressure shifts of the UV absorption edge and the bands ν_{II} and ν_{III} reflect the decrease of the mean O–Mn^{3+} distance with pressure whereas the decrease in the energy difference between ν_{III} and ν_{II} indicates a decreasing distortion of M3 (Langer 1990). Because the experimental setup did not allow measuring the absorption maximum of the band ν_I as a function of pressure, Langer (1990) was not able to calculate the pressure dependence of the crystal field splitting Δ_{oct} for Mn^{3+} in M3.

Spectra of tawmawite. Burns and Strens (1967) recorded the polarized absorption spectra of a natural tawmawite with 0.51 Cr^{3+} pfu. Each polarization displays two moderately intense bands ν_I and ν_{II} situated in the vicinity of ~16,000 cm^{-1} (ν_I) and 24,000 (ν_{II}) (Fig. 6). The absorption maxima of these bands occur at slightly different wavenumbers in the different polarizations. The molar extinction coefficients ε of the observed bands are small (ε ~ 30 l $mole^{-1}$ cm^{-1}) compared to that of the bands arising from Mn^{3+} (ε ~ 100 to 140 l $mole^{-1}$ cm^{-1}; Burns and Strens 1967). From these small molar extinction coefficients and the fact

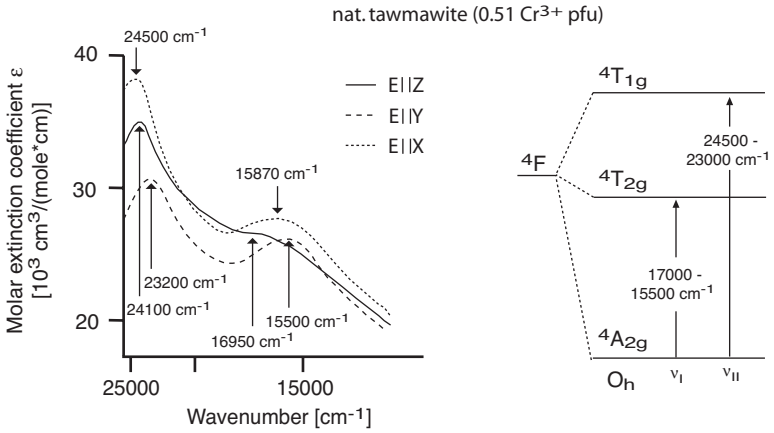

Figure 6. Polarized room temperature spectra of a natural Cr^{3+} epidote ("tawmawite") and the corresponding energy level diagram. Redrawn and modified after Burns and Strens (1967).

that the absorption maxima of the bands occur at not widely separated wavenumbers in the different polarizations, Burns and Strens (1967) concluded that the Cr^{3+} ion substitutes in the centrosymmetric M1 site with D_{2h} site symmetry.

Burns and Strens (1967) assigned the observed bands to the spin allowed *dd* transitions ${}^4A_{2g} \rightarrow {}^4T_{2g}$ (${}^4F$) (band ν_I) and ${}^4A_{2g} \rightarrow {}^4T_{1g}$ (${}^4F$) (band ν_{II}) (Fig. 6). From the position of ν_I, Burns and Strens (1967) calculated a crystal field splitting Δ_{oct} for Cr^{3+} in M1 of 16,225 to 16,410 cm^{-1} and a $CFSE_{Cr3+(M1)}$ of 19,470 to 19,692 cm^{-1} or 233 to 236 kJ/g-atom. However, the combination of the derived Δ_{oct} with the position of ν_{II} results in a Racah parameter B that is higher than that of the free Cr^{3+} ion and therefore physically senseless. The interpretation of the spectra by Burns and Strens (1967) is thus at least questionable.

Optical absorption spectra of the orthorhombic epidote minerals

Spectra of natural and synthetic Mn bearing zoisite ("thulite"). Polarized room temperature absorption spectra of natural and synthetic Mn^{3+} bearing zoisite (variety "thulite") are reported by Petrusenko et al. (1992) in the spectral range 25,000 to 5,000 cm^{-1} and by Langer et al. (2002) in the spectral range 35,000 to 5,000 cm^{-1}. The spectra of Mn^{3+} in zoisite closely resemble those of Mn^{3+} in piemontite and like these they are characterized by a slightly polarized absorption edge in the UV and three intense and strongly polarized bands in the spectral range 30,000 to 10,000 cm^{-1} labeled ν_I, ν_{II}, and ν_{III} (Fig. 7a,b). Like in piemontite, the strong polarization of ν_I, ν_{II}, and ν_{III} accounts for the trichroic scheme of Mn^{3+} zoisite with **X** = light greenish, **Y** = lilac rose, and **Z** = light yellow (Langer et al. 2002). The close similarity

Figure 7 (*on facing page*). (A) Polarized room-temperature absorption spectra of natural Mn^{3+} zoisite ("thulite"). Like in piemontite, the bands ν_I, ν_{II}, and ν_{III} arise from spin allowed *dd* transitions. (B) Polarized room-temperature absorption spectra of synthetic Mn^{3+} zoisite ("thulite"). Beside the bands ν_I, ν_{II}, and ν_{III} (solid arrows) the stippled arrow denotes a band that arises from a spin forbidden *dd* transition of Mn^{3+} in M3 (compare Fig. 2). (C) Polarized absorption spectra of untreated and heat treated natural V^{3+} zoisite ("tanzanite"). On heating the pronounced band at ~22,500 cm^{-1} in the Z-spectrum disappears. (D) Unpolarized absorption spectrum of an untreated natural V^{3+} zoisite ("tanzanite"). The spectrum shows an additional band at ~27,000 cm^{-1} and like the heat-treated specimen in (C) lacks the pronounced band at ~22,500 cm^{-1}. (E) Unpolarized absorption spectra of natural Cr^{3+} zoisite. The two envelopes centered at ~21,800 cm^{-1} and ~15,000 cm^{-1} are due to spin allowed *dd* transitions of Cr^{3+}. The stippled arrows denote bands that arise probably from spin forbidden *dd* transitions of Fe^{3+}. Redrawn and modified after Faye and Nickel (1971), Schmetzer and Berdesinski (1978), and Langer et al. (2002).

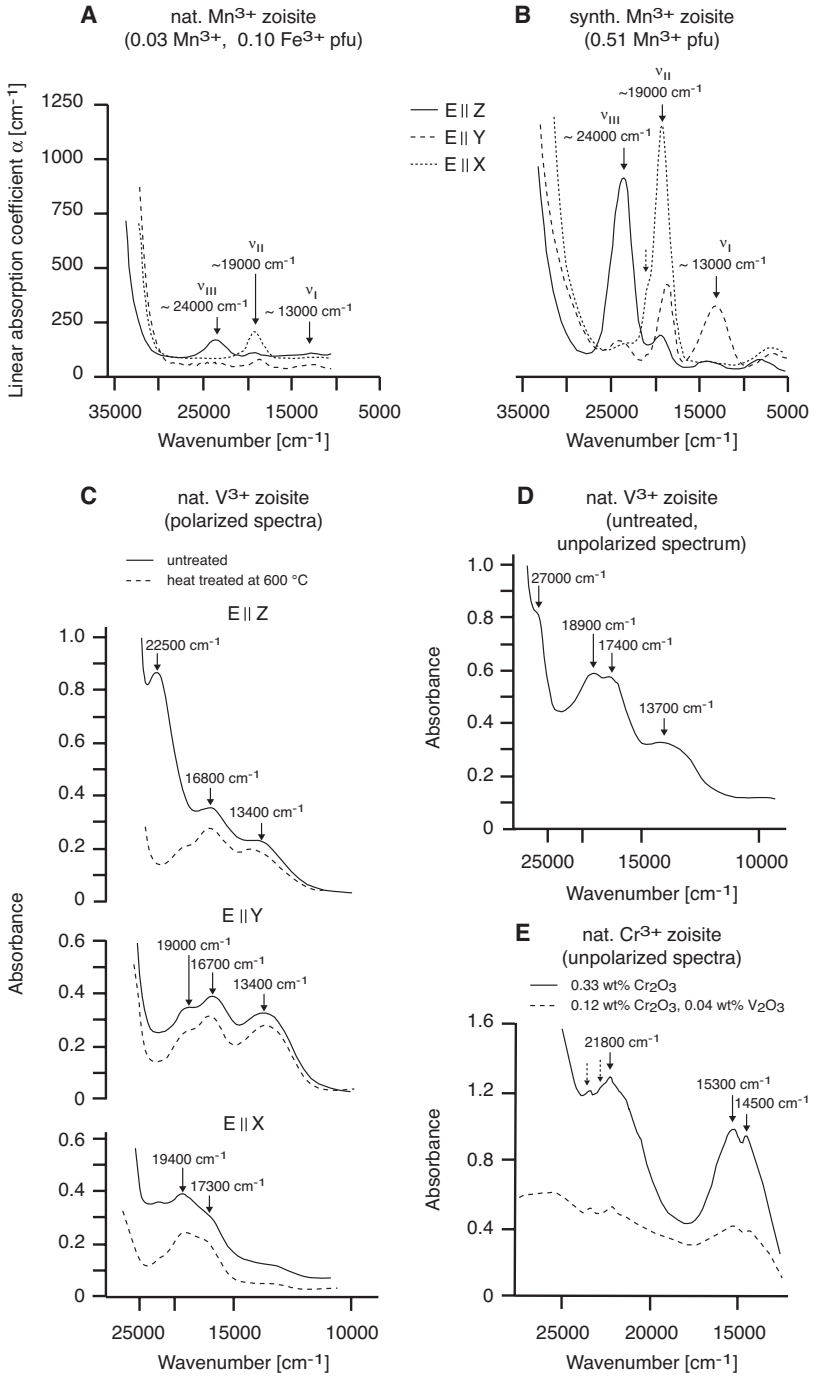

Figure 7. *caption on facing page*

between the spectra of Mn in zoisite and piemontite proves the trivalent state of Mn in zoisite (Kersten et al. 1988; Langer et al. 2002). Due to the different orientation of the indicatrix axes **X** and **Z** with respect to the M3 octahedron in Mn^{3+} zoisite compared to piemontite (see Figs. 16 and 21 of Franz and Liebscher 2004), the polarization of the bands ν_I (Y-spectrum >> X- and Z-spectrum), ν_{II} (X-spectrum >> Y-spectrum > Z-spectrum), and ν_{III} (Z-spectrum >> X- and Y-spectrum) in Mn^{3+} zoisite differ from that in piemontite but their relative intensities are identical to those found in piemontite (compare Fig. 7a,b with Figs 2a, 3). However, the positions of the absorption edge and the absorption maxima of the bands ν_I, ν_{II}, and ν_{III} are at considerable higher wavenumbers than expected from an extrapolation of the piemontite data with respect to Mn^{3+} in M3 (Fig. 4a,b). In Mn^{3+} zoisite ν_I occurs at ~13,000 cm^{-1}, ν_{II} at ~19,000 cm^{-1}, and ν_{III} at ~24,000 cm^{-1} (Fig. 7a,b; Petrusenko et al. 1992; Langer et al. 2002). These higher wavenumbers in Mn^{3+} zoisite are due to the notably smaller mean Mn^{3+}–O distance in Mn^{3+} zoisite compared to piemontite (Langer et al. 2002). Comparing the spectra of synthetic Mn^{3+} zoisite (Fig. 7b) with those of synthetic piemontite (Fig. 3) it is obvious that also the linear absorption coefficient α is distinctly higher in synthetic Mn^{3+} zoisite than expected from an extrapolation of the piemontite data with respect to Mn^{3+} in M3 (Fig. 4a). Langer et al. (2002) ascribe this difference to the different distortion of the M3 octahedron in Mn^{3+} zoisite compared to piemontite. In both structure types the M3 octahedron has site symmetry *m*, but the mean quadratic elongation λ_{oct} and the bond angle variance σ_{oct}^2 (Robinson et al. 1971) significantly differ. Based on their derived structural data, Langer et al. (2002) calculated λ_{oct} = 1.0211 and σ_{oct}^2 = 29.1 for Mn^{3+} zoisite and λ_{oct} = 1.0349 and σ_{oct}^2 = 83.7 for piemontite. From the positions of the absorption maxima of the bands ν_I, ν_{II}, and ν_{III}, Langer et al. (2002) calculated a crystal field splitting Δ_{oct} for Mn^{3+} in M3 in the studied synthetic Mn^{3+} zoisite of 13,780 cm^{-1} corresponding to a CFSE of 14,790 cm^{-1} or 176.9 kJ/g-atom (Fig. 4c). These values are slightly higher than those expected from the extrapolation of the piemontite data (Fig. 4c).

Like the Z-spectrum in synthetic piemontite (Fig. 2a), the X-spectrum of synthetic Mn^{3+} zoisite displays a weak but distinct shoulder at ~20,000 cm^{-1} on the high wavenumber side of the ν_{II} band (Fig. 7b). As Mn^{3+} is confined exclusively to M3 in zoisite, this band must arise from a spin forbidden *dd* transition in Mn^{3+} in M3 (Langer et al. 2002). This spin forbidden *dd* transition is also found in the spectra of a natural Mn^{3+} zoisite reported by Petrusenko et al. (1992). These latter spectra also show an additional weak but distinct band at ~22,000 cm^{-1}. Like in the natural piemontite studied by Smith et al. (1982) this band may be assigned to the spin forbidden ${}^6A_{1g} \rightarrow {}^4A_{1g}, {}^4E_g$ (${}^4G$) transition in Fe^{3+}.

Spectra of V bearing zoisite ("tanzanite"). Optical absorption studies of V bearing zoisite (variety "tanzanite") aimed primarily at elucidating the valence state of the V ion in octahedral coordination and the peculiar color change observed in V zoisite upon heating. Polarized and unpolarized spectra of natural V bearing zoisite specimens are reported by Tsang and Ghose (1971) and Faye and Nickel (1971). The latter studied a tan and a blue colored (in unpolarized white light) specimen. The tan colored specimen contains 0.24 to 0.30% V and ~0.04% Ti, lacks Fe and Mn, and is trichroic in polarized light (before heat treatment), whereas the blue colored specimen contains ~0.19% V, lacks Ti, Fe, and Mn, and is dichroic in polarized light. In case of the tan colored specimen, Faye and Nickel (1971) recorded polarized absorption spectra between 25,000 and 10,000 cm^{-1} before and after heat treatment at 600°C. The polarized spectra of the untreated tan colored specimen are characterized by two broad multi-component envelopes centered at ~13,400 cm^{-1} (Y- and Z-spectrum) and ~18,000 cm^{-1} (X-, Y-, and Z-spectrum), and a strongly polarized band at ~22,500 cm^{-1} (Z-spectrum) (Fig. 7c). These absorption characteristics in the VIS region account for the trichroic scheme observed in the untreated tan colored specimen with **X** = red-violet, **Y** = blue, and **Z** = yellow-green. The X- and Y-spectrum of the heat-treated specimen closely resemble those of the untreated specimen whereas the Z-spectrum of the heat-treated specimen lacks the pronounced band at ~22,500 cm^{-1} (Fig. 7c). As the Z-spectrum of the heat-treated specimen is essentially identical to the Y-

spectrum, this accounts for the change in the pleochroic scheme from trichroic in the untreated specimen to dichroic in the heat-treated specimen with **X** = red-violet, **Y** = **Z** = blue (Faye and Nickel 1971). The unpolarized spectra of both the tan colored (not shown in Fig. 7c) and blue colored (Fig. 7d) specimens extend into the UV region and display a fifth band at ~27,000 cm^{-1} (Faye and Nickel 1971). Beside this band at ~27,000 cm^{-1}, the unpolarized spectrum of the blue colored specimen shows two broad multi-component envelopes at ~13,700 and 18,000 cm^{-1} in good agreement with the polarized spectra of the heat-treated specimen (Fig. 7c,d).

Except the band at ~22,500 cm^{-1}, Faye and Nickel (1971) attribute the observed bands to spin allowed *dd* transitions in V^{3+} and assign the broad multi component envelopes centered at ~13,500 and ~18,000 cm^{-1} to the ${}^3T_{1g} \rightarrow {}^3T_{2g}$ (${}^3F$) and ${}^3T_{1g} \rightarrow {}^3T_{1g}$ (${}^3P$) transitions and the band at 27,000 cm^{-1} to the ${}^3T_{1g} \rightarrow {}^3A_{2g}$ (${}^3F$) transition. The band at ~22,500 cm^{-1} is the only one that is affected by heat treatment and it is therefore unlikely that it comprises a part of the *dd* spectrum of V^{3+}. As V and Ti are the only transition metal ions present in the tan colored specimen, Faye and Nickel (1971) assign this band to the ${}^2T_{2g} \rightarrow {}^2E_g$ transition in either V^{4+} or Ti^{3+}, however favor Ti^{3+} because of its charge and because the band at ~22,500 cm^{-1} is only found in the Ti bearing specimen. A $Ti^{3+} \rightarrow Ti^{4+}$ charge transfer that is proposed responsible for the pleochroism of Ti bearing andalusite by Faye and Harris (1969) can be ruled out in case of zoisite as the polarization of the band at ~22,500 cm^{-1} can neither be related to the M1,2–M3 nor the M1,2–M1,2 vector between adjacent octahedral sites. The disappearance of the band at ~22,500 cm^{-1} on heating suggests the oxidation of Ti^{3+} to Ti^{4+} or of V^{4+} to V^{5+}. As both Ti^{4+} and V^{5+} have a d^0 configuration, they do not give rise to any *dd* absorption spectrum. However, because the band at ~22,500 cm^{-1} disappears on heating in air as well as in hydrogen the proposed oxidation of Ti^{3+} or V^{4+} would occur in an oxidizing as well as in a reducing environment and Faye and Nickel (1971) state that "it is difficult to rationalize a mechanism that accounts for this proposal." Based on their data, Faye and Nickel (1971) conclude that V^{3+} is strongly ordered in the M3 site whereas Ti^{3+} is probably ordered in M1,2. Contrary, Tsang and Ghose (1971) conclude that V^{3+} is approximately randomly distributed between M1,2 and M3.

Spectra of Cr^{3+} bearing zoisite. Studies of Cr^{3+} in zoisite are restricted to the remission and absorption spectra of natural Cr^{3+} bearing zoisite recorded by Schmetzer and Berdesinski (1978). The unpolarized absorption spectra of two polycrystalline samples are characterized by two broad bands centered at ~15,100 cm^{-1} (ν_I) and ~21,800 cm^{-1} (ν_{II}) (Fig. 7e) resembling the principal features of the tawmawite spectra (see Fig. 6). Additional weak bands or shoulders can be identified on the high wavenumber side of ν_{II} at ~23,400 and 22,100 cm^{-1} whereas ν_I is clearly split into two components at 15,300 and 14,500 cm^{-1} (Fig. 7e). Schmetzer and Berdesinski (1978) assigned the bands ν_I and ν_{II} to the spin allowed ${}^4A_{2g} \rightarrow {}^4T_{2g}$ and ${}^4A_{2g} \rightarrow {}^4T_{1g}$ transitions in Cr^{3+}. The weak features at ~23,400 and 22,100 cm^{-1} are most probably due to spin forbidden *dd* transitions in Fe^{3+} whereas the fine structure of the band ν_I is either due to a splitting of the ${}^4A_{2g} \rightarrow {}^4T_{2g}$ transition or to an overlap with the spin forbidden ${}^4A_{2g} \rightarrow {}^2T_{1g}$, ${}^2E_g$ transition in Cr^{3+} (Schmetzer and Berdesinski 1978). From the center of the band ν_I Schmetzer and Berdisinski (1978) calculated a crystal field splitting Δ_{oct} of 15,100 cm^{-1} for Cr^{3+} in zoisite, which is lower than that derived for Cr^{3+} in tawmawite (~16,300 cm^{-1}, see above; Burns and Strens 1967). The low Δ_{oct} suggests a strong preference of Cr^{3+} for the M3 compared to the M1,2 site in zoisite as the smaller mean O–M distance in M1,2 would result in a higher Δ_{oct} (Schmetzer and Berdisinski 1978).

INFRARED SPECTROSCOPY

Moenke (1962) published a first infrared (IR) spectrum of an epidote. Polarized single crystal IR spectroscopy focused on the determination of the proton location within the monoclinic and orthorhombic crystal structures (Hanisch and Zemann 1966; Linke 1970).

The first systematic study on the spectral properties in the spectral range 5,000 to 250 cm^{-1} of the monoclinic and orthorhombic Al-Fe^{3+} solid solution series as function of the Fe^{3+} content stems from Langer and Raith (1974). The spectrum of a deuterated zoisite was presented by Langer and Lattard (1980), and Winkler et al. (1989) studied the influence of pressure on the OH environment in zoisite. Janeczek and Sachanbinski (1989) report the IR spectrum of an Mn bearing clinozoisite. Later, Gavorkyan (1990) and Petrusenko et al. (1992) studied a suite of natural epidote minerals including zoisite, clinozoisite, Mn bearing clinozoisite, epidote, and allanite by IR spectroscopy and published the first IR spectrum of a deuterated clinozoisite. The structural changes of the OH environment that accompany the incorporation of Sr in the A sites and of Mn^{3+} in the M3 site in the monoclinic solid solution series has then been studied by Della Ventura et al. (1996). The systematic work of Langer and Raith (1974) was extended by Heuss-Aßbichler (2000) for the monoclinic series and by Brunsmann (2000) and Liebscher et al. (2002) for the orthorhombic series. Bradbury and Williams (2003) used pressure dependent infrared spectroscopy to study the response of the monoclinic structure to changes in pressure with special emphasis given to the bonding environment of the hydrogen. Recently, Liebscher and Gottschalk (2004) studied the temperature evolution of the IR spectra of zoisite. IR spectra of allanite were recorded by Cech et al. (1972), Mingshen and Daoyuan (1986), and Mingshen and Dien (1987). Cech et al. (1972) compared the spectrum of allanite with that of an epidote whereas Mingshen and Daoyuan (1986) and Mingshen and Dien (1987) studied the evolution of the allanite IR spectrum with the degree of metamictization.

IR spectroscopy of monoclinic epidote minerals

All published IR spectra of the monoclinic epidote minerals are consistent with respect to their general features. They are characterized by the main OH stretching vibration between about 3,450 and 3,300 cm^{-1} (depending on composition) and the lattice vibrations below about 1,200 cm^{-1}. Langer and Raith (1974) identified a total of 34 bands in the studied spectral range of 5,000 to 200 cm^{-1} and numbered them consecutively from high to low wavenumber. This numbering is also adopted here. Band 1 corresponds to the main OH stretching vibration whereas the bands 2 to 34 correspond to vibrations below 1,200 cm^{-1}. It should be noted that Le Cleac´h et al. (1988) observed the lowest IR active mode in clinozoisite at 80 cm^{-1}.

Lattice vibrational range. Typical room temperature powder (KBr pellets) IR spectra below 1,200 cm^{-1} of natural and synthetic Al-Fe^{3+} solid solutions with Fe^{3+} contents between X_{Ep} = 0.00 and X_{Ep} = 0.98 from Langer and Raith (1974) and Heuss-Aßbichler (2000) are shown in Figure 8. They are characterized by strong absorption (Fig. 8a) and low transmission (Fig. 8b), respectively, between about 1,200 and 820 cm^{-1} (bands 2 to 12) and below about 700 cm^{-1} (bands 14 to 34; Fig. 8). Between about 820 and 700 cm^{-1} there is only one very weak band (band 13) present in the monoclinic epidote minerals independent on Fe content. This is in contrast to the orthorhombic forms, which show two sharp bands of medium intensity in this region (see below). In the 1,200 to 820 cm^{-1} range the bands 5, 7, and 9 occur as single marked bands throughout the entire compositional range whereas bands 6, 8, 10, 11, and 12 only show up as weak to very weak shoulders of the main bands (Fig. 8). Bands 2, 3, and 4 partly strongly overlap and display noticeable changes with increasing Fe content. Band 2 can be traced throughout the entire compositional range whereas the bands 3 and 4 significantly change their relative intensities. From these two bands only band 3 can be resolved as single band in Fe free clinozoisite, band 4 is either absent or its intensity is to low to be resolved (Fig. 8b, lowermost spectrum). With increasing Fe content the intensity of band 4 increases whereas that of band 3 decreases. Consequently, in medium Fe clinozoisite–epidote both bands strongly overlap, display a comparable intensity, and occur as shoulders of band 2 (spectra with X_{Ep} = 0.39, 0.44, and 0.48 in Fig. 8). In Fe rich epidote the band 4 shows up as a single band whereas band 3 cannot be resolved with confidence due to the strong overlap of bands 2 and 4 (spectra with $X_{Ep} > 0.72$ in Fig. 8) and might even be absent in the most Fe rich samples.

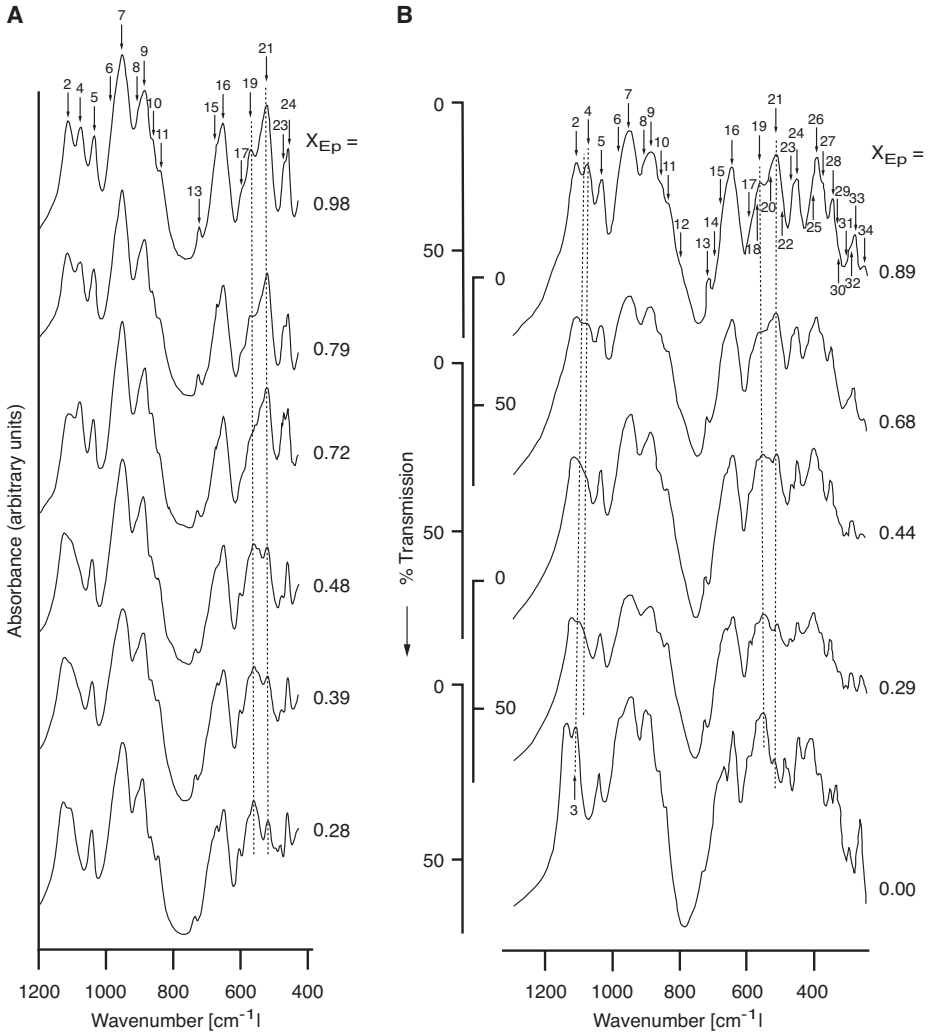

Figure 8. Typical IR spectra of monoclinic Al-Fe^{3+} solid solutions with different iron contents from (A) Heuss-Aßbichler (2000) and (B) Langer and Raith (1974). Note that the spectra in (A) are displayed in the form of absorbance whereas those in (B) are displayed in the form of transmission. To allow for easier visual comparison between (A) and (B) the spectra in (B) are shown in an unconventional orientation with the transmission increasing downwards. Dotted lines correspond to IR bands that significantly change with increasing iron content and that are discussed in detail in the text. Redrawn and modified after Langer and Raith (1974) and Heuss-Aßbichler (2000).

Below 700 cm^{-1} the spectra of monoclinic Al-Fe^{3+} solid solutions remarkably change with increasing Fe content and only the bands 13, 16, 26, and 28 can be confidentially resolved as single bands throughout the entire compositional range (Fig. 8). Like the bands 3 and 4 some of the bands below 700 cm^{-1} significantly change their relative intensities. Band 21 occurs only as a shoulder of the much more intense bands 19 and 20 at low Fe contents but is one of the most prominent bands below 700 cm^{-1} in Fe rich epidote. In these Fe rich epidotes bands

19 and 20 only show up as shoulders of band 21 (Fig. 8). Band 22 is a single sharp band of medium intensity in Fe free clinozoisite (lowermost spectra of Fig. 8b) but occurs as a weak shoulder of band 21 at high Fe content. Likewise, band 23 is a weak shoulder of band 22 in Fe free clinozoisite, a single sharp band of low intensity in medium Fe clinozoisite–epidote, and occurs as a shoulder of band 24 in Fe rich epidote (Fig. 8). Band 29 can be resolved as a single band in Fe free clinozoisite with an intensity slightly higher than that of band 28 (lowermost spectra of Fig. 8b). With increasing Fe content the intensity of band 29 decreases relative to that of band 28 and already at an Fe content of $X_{Ep} = 0.29$ band 29 occurs only as a shoulder of band 28. The bands 32, 33, and 34 display a similar change in their relative intensities. In Fe free clinozoisite band 34 is very sharp and pronounced compared to the low intensity maximum which is formed either by band 32 or 33 (Langer and Raith 1974 were not able to unequivocally assign this low intensity maximum to one of these two bands). With increasing Fe content the intensity of band 34 significantly decreases relative to the intensity of bands 32 and 33. In Fe rich epidote the bands 32 and 33 can be resolved as individual bands of medium intensity whereas band 34 only occurs as a band of low intensity (uppermost spectra in Fig. 8b).

Those bands that can be confidentially resolved as single bands throughout the entire compositional range (bands 5, 7, 9, 13, 16, 26, and 28) either shift to lower wavenumber with increasing Fe content (bands 5, 9, 13, 26, and 28) or display a constant position over the entire compositional range (bands 7 and 16; Fig. 9a; see also Fig. 4 of Langer and Raith 1974). The shift to lower wavenumber of the bands 5, 9, 13, 26, and 28 can well be used to estimate the Fe content of monoclinic Al-Fe^{3+} solid solutions from IR spectra. Linear regressions relating band position to Fe content show two groups of bands with different slopes (Fig. 9a; see also Table 5 of Langer and Raith 1974). The bands 5 and 9 (Fig. 9a) and 28 ($\nu = 364.2 - 13.2X_{Ep}$; Langer and Raith 1974) display negative slopes of −12.5 to −13.2 whereas the bands 13 (Fig. 9a) and 26 ($\nu = 419.4 - 27.2X_{Ep}$; Langer and Raith 1974) have steeper negative slopes of −23.8 to −27.2. According to Langer and Raith (1974) the determination of the Fe content using these linear correlations is accurate to about ±0.04 X_{Ep} for bands 13 and 26 and about ±0.08 X_{Ep} for bands 5, 9, and 28.

Bradbury and Williams (2003) studied the room temperature evolution of the IR spectrum of a clinozoisite with $X_{Ep} = 0.46$ with pressure up to 36 GPa. Within the 1,250 to 550 cm^{-1} spectral region they tracked the evolution of the bands 2, 5, 7, 9, 10, 11, 15, and 16 with pressure (only bands 2, 5, 7, 9, 15, and 16 are shown in Fig. 9b). All bands shift to higher wavenumber with compression in accordance with the anticipated response of vibrations to simple bond compaction. This shift was found to be continuous up to 16 GPa and fully reversible on decompression, indicating that no phase change occurred up to this pressure (Bradbury and Williams 2003). Except band 15 which shows a notably small pressure shift of only 0.6 cm^{-1}/GPa, the rate at which the bands shift upon compression ranges from 3.1 cm^{-1}/GPa (bands 7, 9, and 11) to 4.5 cm^{-1}/GPa (bands 2 and 16) and is in general accord with the pressure shift of stretching vibrations in other ortho- and sorosilicates (Bradbury and Williams 2003). From the band positions (ω_0) at ambient pressure, the shift of the bands with pressure ($d\omega/dP$), and the bulk moduli (K_0) for clinozoisite from Holland et al. (1996; $K_0 = 154$ GPa) and Comodi and Zanazzi (1997; $K_0 = 127$ GPa) Bradbury and Williams (2003) calculated the Grüneisen parameter $\gamma = (K_0/\omega_0)(d\omega/dP)$ for each band. The small pressure shift of band 15 corresponds to a small Grüneisen parameter of only 0.12 (for $K_0 = 127$ GPa) and 0.14 (for $K_0 = 154$ GPa). Depending on the bulk modulus chosen, the other bands have Grüneisen parameters between 0.41 (band 7, calculated for $K_0 = 127$ GPa) and 1.04 (band 16, calculated for $K_0 = 154$ GPa). The average mode Grüneisen parameter is 0.48 for $K_0 = 127$ GPa and 0.58 for $K_0 = 154$ GPa. For comparison, Bradbury and Williams (2003) calculated a bulk thermodynamic Grüneisen parameter from $\gamma = \alpha K_0/\rho C_P$ with the data for α and C_P from Pawley et al. (1996) and Kiseleva and Ogorodnikova (1987), respectively. With $\gamma = 0.75$ for $K_0 = 127$ GPa and $\gamma = 0.91$ for $K_0 = 154$ GPa, the bulk thermodynamic Grüneisen parameter is slightly higher than the average

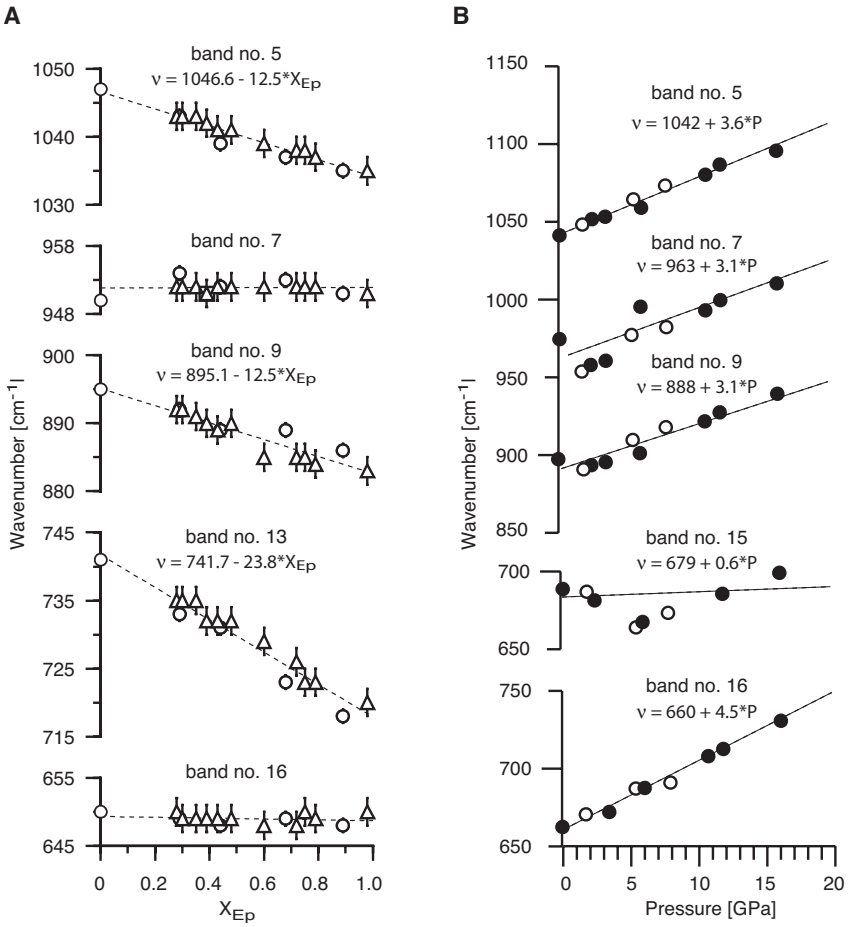

Figure 9. Compositional (A) and pressure (B) shifts of some IR bands in the lattice vibrational range of monoclinic Al-Fe^{3+} solid solutions. (A) The bands either shift to lower wavenumber with increasing iron content or display a constant position over the entire compositional range. The equations that relate the band positions to the iron content represent linear fits to the data points. Data sources for (A) are: ○ = Langer and Raith (1974), △ = Heuss-Aßbichler (2000). (B) Except for band 15, which shows a comparable small pressure shift, the bands shift to higher wavenumber with pressure with a slope of about 3.1 to 4.5 cm^{-1}/GPa. The equations are linear fits to the data. In (B), ● represent data that were determined during compression, ○ are data that were determined during decompression (redrawn and modified after Bradbury and Williams 2003).

mode Grüneisen parameter derived from the mid infrared modes. This indicates that bands that were not observed by Bradbury and Williams (2003) either at lower frequencies, in the Raman spectrum, or off-Brillouin zone center modes must have larger average Grüneisen parameters than the observed ones (Bradbury and Williams 2003).

Band assignment. Up to now, no rigorous band assignment has been performed for the lattice vibrational range of the spectra of monoclinic epidote minerals. Langer and Raith (1974) assigned the bands 2, 3, 5, 7, 9, 11, and 16 to Si–O valence vibrations of the single SiO_4 tetrahedron or the Si_2O_7 group. Bradbury and Williams (2003) adopted these assignments

except for band 16 and assigned additionally band 10 to a Si–O valence vibration. Contrary to Langer and Raith (1974), Bradbury and Williams (2003) assigned band 16 to either an Al–O stretching or a Si–O bending vibration. The spectral evolution of the bands 3 and 4 (see above) sheds additional light on the interpretation of these two bands. It is reasonable to assume that not only band 3 but also band 4 is due to a Si–O valence vibration. As band 4 is missing in the spectrum of Fe free clinozoisite and its intensity increases with increasing Fe content whereas that of band 3 decreases, both bands should arise from a Si–O bond that is influenced by the substitution of Fe^{3+} in a neighboring octahedron. The most likely candidate is the Si2–O8–M3 bridge with bands 3 and 4 representing the Si2–O8 valence vibration for Al and Fe^{3+} in M3, respectively. This interpretation was already discussed by Heuss-Aßbichler (2000).

By analogy with some layer silicates, band 8 was interpreted as due to an OH bending vibration by Langer and Raith (1974). Because of its small pressure shift, Bradbury and Williams (2003) assigned band 15 to an OH bending vibration. Gavorkyan (1990) and Petrusenko et al. (1992) observed additional bands at 780 and 665 cm^{-1} in synthetic fully deuterated clinozoisite that are missing in the spectra of undeuterated clinozoisite and therefore arise from OD bending vibrations. Taking a ν_{OH}/ν_{OD} factor of 1.34 to account for the isotope effect, Petrusenko et al. (1992) calculated the corresponding OH bending vibrations in the undeuterated form to occur at about 1045 and 890 cm^{-1}. These values closely correspond to the positions of the bands 5 and either band 8 or 9. The interpretation of band 5 as arising from an OH bending vibration is in contradiction to the interpretation of this band as due to a Si–O valence vibration by Langer and Raith (1974) and Bradbury and Williams (2003). In the spectrum of the fully deuterated clinozoisite (Gavorkyan 1990; Petrusenko et al. 1992) band 5 still appears but with a significantly smaller intensity as in the spectra of the undeuterated forms. Band 5 therefore most probably originates from two strongly overlapping bands that are due to an OH bending and a Si–O valence vibration of almost identical energy. The occurrence of an OH bending vibration at about 890 cm^{-1} agrees well with the interpretation of Langer and Raith (1974), although it is not clear from the data, which of the two bands 8 and 9 actually correspond to the second OH bending vibration. The interpretation of band 15 as due to an OH bending vibration by Bradbury and Williams (2003) could not be verified by the work of Gavorkyan (1990) and Petrusenko et al. (1992).

As the spectra of monoclinic and orthorhombic epidote minerals are completely different between 820 to 700 cm^{-1} and 540 to 320 cm^{-1} (see below), bands in these spectral regions most probably originate from M–O vibrations within the different octahedra of the two structure types (Langer and Raith 1974). Only band 34 of the monoclinic epidote minerals has an equivalent in the orthorhombic structure (band 48, see below) and was thus assigned to a Ca–O vibration by Langer and Raith (1974).

OH stretching vibrational region. In the monoclinic Al-Fe^{3+} solid solutions the OH stretching vibration occurs between 3,330 and 3,380 cm^{-1} (Figs 10a,b and 11a; Langer and Raith 1974; Della Ventura et al. 1996; Heuss-Aßbichler 2000) and is characterized by the single sharp band 1 (nomenclature of Langer and Raith 1974). Hanisch and Zemann (1966) measured the pleochroic scheme of the OH stretching vibration in epidote by means of polarized single crystal IR spectroscopy and observed the maximum absorption parallel [001] and minor absorption parallel [100] and [010] with the absorption parallel [100] being slightly larger than parallel [010]. They described the three dimensional absorption figure of the OH stretching vibration as a lemniscate that rotates around [001] and confirmed the bonding of the proton to O10 with a hydrogen bridge to O4 as already proposed by earlier structure refinement studies (e.g., Ito et al. 1954; Belov and Rumanova 1954). The data from Langer and Raith (1974) and Heuss-Aßbichler (2000) show that the OH stretching vibration of Al-Fe^{3+} solid solutions correlates linearly with the Fe content according to $\nu = 3{,}327.1 + 49.4\ X_{Ep}$ (Fig. 11a). The determination of the Fe content in Al-Fe^{3+} solid solutions with this band is accurate to about ± 0.04 X_{Ep} (Langer and Raith 1974).

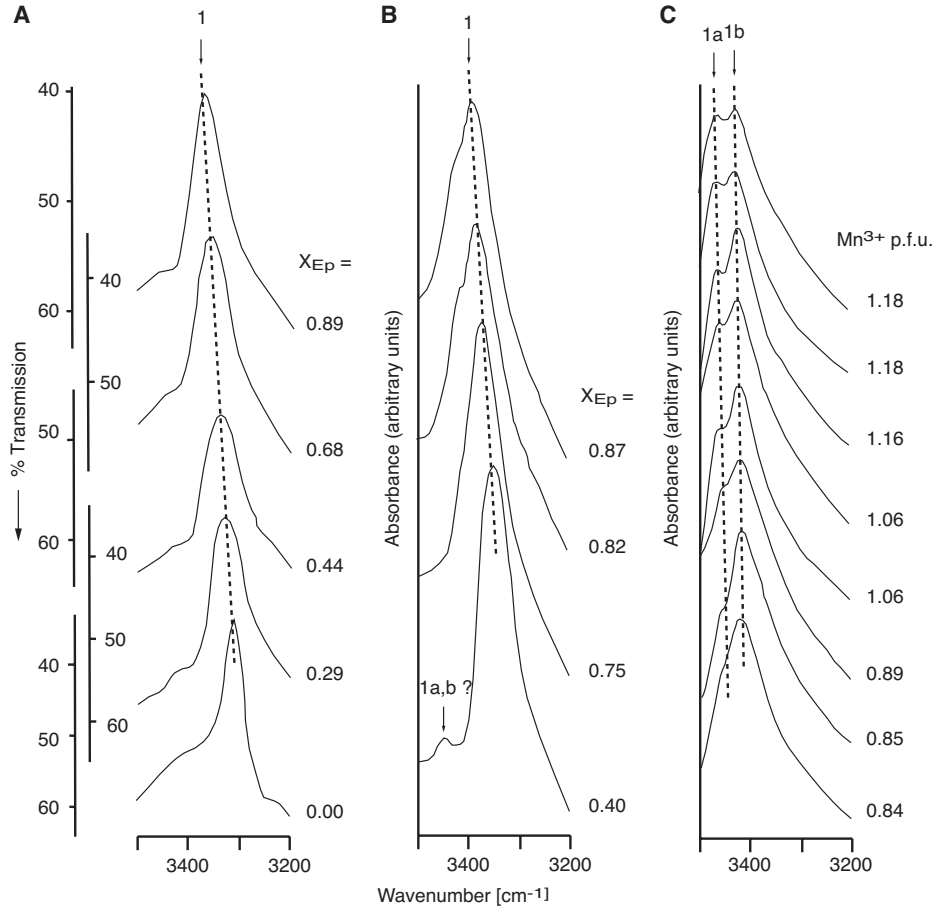

Figure 10. Typical IR spectra of monoclinic Al-Fe^{3+} solid solutions (A), (B) and of piemontites (C) in the region of the OH stretching vibration. Note that the spectra are displayed in the form of transmission in (A) and in the form of absorbance in (B) and (C). Like in Figure 8, the spectra in (A) are shown in an unconventional orientation with the transmission increasing downwards. In the monoclinic Al-Fe^{3+} solid solutions the OH stretching vibration is characterized by a single sharp maximum between about 3380 and 3330 cm^{-1}. The spectra of piemontite (C) show a splitting of the main OH stretching vibration into two components 1a and 1b and a significant shift to higher wavenumber (about 3460 to 3410 cm^{-1}) compared to the Al-Fe^{3+} solid solutions. Redrawn and modified after Langer and Raith (1974) and Della Ventura et al. (1996).

In natural Sr bearing piemontite samples with 0.836 to 1.197 Mn^{3+} pfu, 0.056 to 0.379 Fe^{3+} pfu, and 0.09 to 0.291 Sr pfu, Della Ventura et al. (1996) found a shift of the OH stretching vibration to significantly higher wavenumbers compared to the Al-Fe^{3+} solid solution series as well as a splitting of the main band into two components. Such a splitting was also observed by Langer et al. (1976) in synthetic piemontite with more than about 1.0 Mn^{3+} pfu. To be in line with the numbering of Langer and Raith (1974) these two components are labeled as bands 1a and 1b (Fig. 10c). Independent on composition the band separation between bands 1a and 1b is 35 to 40 cm^{-1} (Fig. 11a). Band 1b is the main component and appears as a sharp maximum in all spectra. It occurs between 3,412 and 3,423 cm^{-1}. Band 1a is the higher energy component

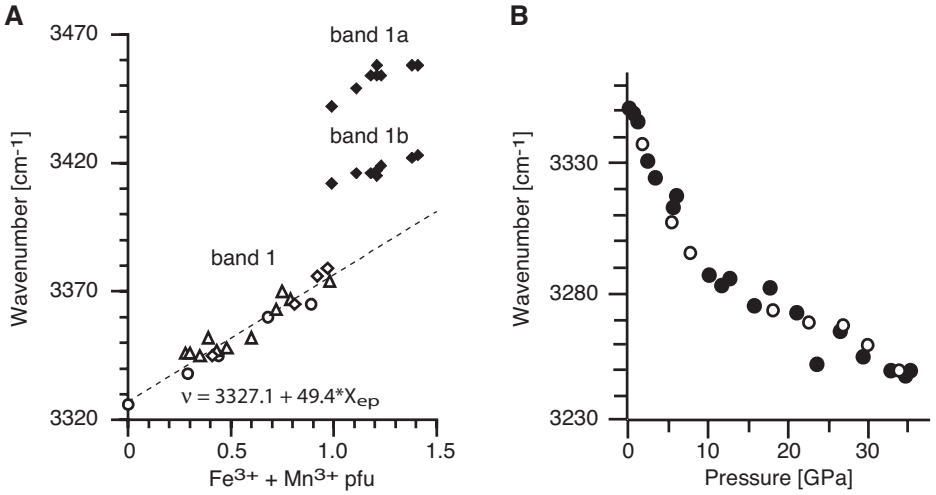

Figure 11. Compositional (A) and pressure (B) shifts of the OH stretching vibrations of monoclinic epidote minerals. (A) Band 1 of the monoclinic Al-Fe^{3+} solid solutions (open symbols) shifts linearly to higher wavenumber with increasing iron content. The stippled line represents a linear fit to the data. In piemontite (filled symbols) band 1 is splitted into the two bands 1a and 1b that also shift to higher wavenumber with increasing iron content although with a slightly smaller compositional dependence. The band separation between bands 1a and 1b is about 35 to 40 cm^{-1} in all samples. Circles are from Langer and Raith (1974), triangles from Heuss-Aßbichler (2000), and diamonds from Della Ventura et al. (1996). (B) Band 1 of monoclinic Al-Fe^{3+} solid solutions generally shifts to lower wavenumber with pressure but shows a break in slope at about 15 GPa. Below 15 GPa the shift is −5.1 cm^{-1}/GPa, above 15 GPa the average shift is only −1.5 cm^{-1}/GPa. Filled circles represent data that were determined during compression, open circles data that were determined during decompression (data are for a clinozoisite with X_{Ep} = 0.46; redrawn after Bradbury and Williams 2003).

and occurs between 3,442 and 3,458 cm^{-1} (Figs 10c, 11a). With increasing Mn^{3+} content its intensity increases relative to that of band 1b and consequently it occurs as a shoulder at the high energy side of band 1b at low Mn^{3+} content (Mn^{3+} + Fe^{3+} = 0.99 to 1.25 pfu; lower four spectra in Fig. 10c) but forms a medium to sharp maximum at higher Mn^{3+} + Fe^{3+} content (Mn^{3+} + Fe^{3+} = 1.21 to 1.41 pfu; upper four spectra in Fig. 10c). Both bands display a positive linear shift with the Mn^{3+} + Fe^{3+} content of almost identical slope (Figs 10c, 11a).

Assuming only Al in the M2 site, Della Ventura et al. (1996) interpreted the general shift of the OH stretching vibration to higher wavenumber in Sr bearing piemontite as being due to the substitution of Sr for Ca in the A2 site. According to the structural data of Dollase (1969), Catti et al. (1989), Ferraris et al. (1989), and Bonazzi et al. (1990) the incorporation of Sr has a major effect on the expansion of the A2 polyhedron and especially the A2–O10 distance increases linearly with the Sr content at least up to 0.5 Sr pfu in A2 (see Fig. 6 of Della Ventura et al. 1996). The increasing A2–O10 distance leads to a decrease of the incident bond strength at O10 and an increase of the O10–H bond strength and consequently shifts the OH stretching vibration to higher wavenumber (Della Ventura et al. 1996). This interpretation is in accord with the results of Perseil (1987) who found a shift of the OH stretching vibration to higher wavenumber with increasing Sr content in piemontite samples with an identical Mn^{3+} + Fe^{3+} content. The observed splitting of the OH stretching vibration is due to the Jahn-Teller effect that the Mn^{3+} cation exerts on the M3 octahedron (Della Ventura et al. 1996). The substitution of Mn^{3+} for Al in M3 flattens the M3 octahedron along the O4–O8 direction and shortens the M3–O4 bond length compared to the Al-Fe^{3+} solid solution series (see Fig. 5 of Della Ventura

et al. 1996). As a consequence the length of the H…O4 hydrogen bridge increases and the stretching vibration is shifted to a higher wavenumber. Della Ventura et al. (1996) therefore assigned band 1a to the configuration $^{[M2]}Al_2$–O10–H…O4–$^{[M1]}(Al,Fe^{3+})_2{}^{[M3]}Mn^{3+}$. The band separation of 35 to 40 cm^{-1} between the bands 1a and 1b corresponds to a difference in the length of the underlying hydrogen bridge of about 0.02 to 0.03 Å (Bellamy and Owen 1969). This is consistent with the structural data for piemontite that indicate an about 0.04 Å shorter M3–O4 bond length compared to Al-Fe^{3+} solid solutions of comparable substitutional degree (see Fig. 5 of Della Ventura et al. 1996). Based on the spectral properties of the Al-Fe^{3+} solid solutions and piemontite, respectively, Della Ventura et al. (1996) speculated about two different types of behavior of the OH stretching vibration in monoclinic epidote minerals: a continuous shift of a single band in Al-Fe^{3+} solid solutions as a function of the Fe content (their so-called "one-mode behavior") and a splitting of the OH stretching vibration into two separate bands in piemontite as a function of the (Al,Fe^{3+})–Mn^{3+} distribution (their so-called "two-mode behavior"). However, the authors did not exclude a second explanation, i.e., that the OH stretching vibration is also split into two separate bands in the Al-Fe^{3+} solid solutions but that the band separation due to the different octahedral configurations is too small to be resolved in their samples and by their methods, respectively. By analogy with the results of IR studies on the OH stretching vibration in orthorhombic Al-Fe^{3+} solid solutions that show two bands with a small band separation due to the different octahedral configurations (see below), this second explanation seems to be much more likely.

At room temperature the OH stretching vibration shifts to lower wavenumber with increasing pressure whereas the peak markedly broadens (Fig. 11b; Bradbury and Williams 2003 for a clinozoisite with $X_{Ep} = 0.46$). The shift is not linear but shows a break in slope at about 15 GPa: below about 15 GPa it is −5.1 cm^{-1}/GPa whereas the average shift above 15 GPa is only −1.5 cm^{-1}/GPa. For $P < 15$ GPa the corresponding Grüneisen parameter is $\gamma = -0.19$ and −0.23 for a bulk modulus of $K_0 = 127$ and 154 GPa, respectively (for the calculation of γ see above). The shift of the stretching vibration as well as the broadening of the peak are significantly less than those observed by Winkler et al. (1989) for the OH stretching vibration in zoisite (see below). This difference probably reflects the weaker, longer, and more bent hydrogen bond in clinozoisite compared to zoisite, which may be therefore less sensitive to pressure (Bradbury and Williams 2003). But compared to other hydrous phases that have comparable ambient pressure hydrogen bond strengths (e.g., lawsonite, chondrodite, and hydrated β-phase; Williams 1992; Cynn and Hofmeister 1994; Scott and Williams 1999) and compared to its own Si–O stretching vibrations, the broadening of the OH stretching vibration in clinozoisite is markedly larger (Bradbury and Williams 2003).

To explain the shift and the broadening of the OH stretching vibration in clinozoisite with pressure, Bradbury and Williams (2003) modeled its hydrogen bond potential (Fig. 12). At ambient pressure this model describes a double potential well in which the hydrogen atom is preferentially bound to O10 (Fig. 12). With increasing pressure the minimum of the deeper well moves away from O10 and suggests an increasing O10–H bond length with a concomitant decrease in energy, which is in accord with the observed shift of band 1 to lower wavenumber with pressure. Calculating the first excited state of the hydrogen atom as 3/2 the energy of the OH stretching vibration above the well energy minimum (Herzberg 1950; Bradbury and Williams 2003), it is also evident from Figure 12 that the potential well significantly broadens with pressure. This broadening increases the amount of thermal disorder of the hydrogen atom along the axis of the hydrogen bond and is responsible for the broadening of the OH stretch peak in the IR spectra (Bradbury and Williams 2003). Based on the modeled hydrogen bond potential the hydrogen bond in clinozoisite might become symmetric at pressures above 50 GPa.

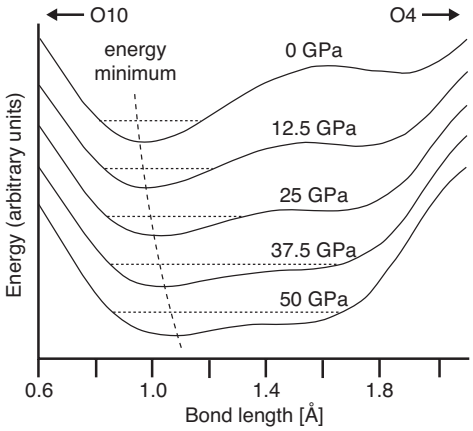

Figure 12. Modeled hydrogen potential for the O10–H…O4 hydrogen bond in monoclinic Al-Fe^{3+} solid solution for different pressures. At low pressure the potential is a double well with one pronounced energy minimum and the proton is preferentially bound to O10. With increasing pressure this minimum moves away from O10 and suggests an increasing O10–H bond length (stippled line). Calculating the first excited state of the proton as 3/2 the energy of the OH stretching vibration above the well energy minimum it is evident that the potential well also significantly broadens with pressure. Redrawn and modified after Bradbury and Williams (2003).

IR spectroscopy of zoisite

Moenke (1962) published a zoisite IR spectrum between 4,000 to 400 cm^{-1}. Later, Linke (1970) studied the proton environment in zoisite by means of polarized single crystal IR spectroscopy and Langer and Raith (1974) investigated systematically the powder IR spectral properties of zoisite and their dependence on composition. They identified a total of 36 bands in the spectral range 5,000 to 200 cm^{-1}. In detailed temperature dependent ($T = -170$ to 250°C) IR spectroscopic studies in the range 5,000 to 350 cm^{-1}, Brunsmann (2000), Liebscher et al. (2002), and Liebscher and Gottschalk (2004) were able to identify 12 additional bands resulting in a total of 48 bands in the spectral range 5,000 to 200 cm^{-1} (Fig. 13). To be in line with the numbering of the bands in the monoclinic epidote minerals and with the numbering introduced by Langer and Raith (1974), these bands will be consecutively numbered from high to low wavenumber. Like the IR spectra of the monoclinic epidote minerals all published IR spectra of different varieties of zoisite resemble each other in their principal features. The IR spectrum is characterized by the OH stretching vibration at 3,300 to 3,000 cm^{-1}, a low intensity band at 2,300 to 2,100 cm^{-1} which is most probably related to an OH bending vibration (see below), and the lattice vibrations below 1,200 cm^{-1}.

Lattice vibrational range. Typical powder IR spectra in the lattice vibrational range below 1,200 cm^{-1} from Langer and Raith (1974) and Liebscher and Gottschalk (2004) are shown in Figure 13. The spectra from Liebscher and Gottschalk (2004) were recorded at −150°C (Fig. 13a) whereas those from Langer and Raith (1974) were recorded at room temperature conditions (Fig. 13b). All spectra are characterized by strong absorption and low transmission, respectively, between about 1,180 and 1,080 cm^{-1} (bands 11 to 13), 1,000 and 800 cm^{-1} (bands 14 to 23), 800 to 720 cm^{-1} (bands 24 and 25), and below 720 cm^{-1} (bands 26 to 48). In the low temperature spectra most of the bands are single sharp maxima of medium to high intensity and only the bands 11, 14, 15, 17, 19, 22, 23, 30, 35, 36, 37, and 42 occur as weak shoulders of the main bands (Fig. 13a). With increasing temperature the bands broaden and strongly overlap and only the main bands are still observable at high temperature (Liebscher and Gottschalk 2004). Already in the room temperature spectra of Langer and Raith (1974) only the bands 24, 25, 26, 27, 31, 38, 40, 41, 46, 47, and 48 are visible as single sharp maxima. Due to this strong overlap, Langer and Raith (1974) were unable to resolve bands 12 and 13 as single bands and erroneously interpreted them to represent only one band (6) and claimed this feature as a main difference to the spectra of monoclinic epidote minerals, in which they were able to recognize two separate maxima in this region (bands 2 and 3 or 4 in Fig. 8). The best suited and most easily recognizable criteria to distinguish between the spectra of monoclinic and orthorhombic

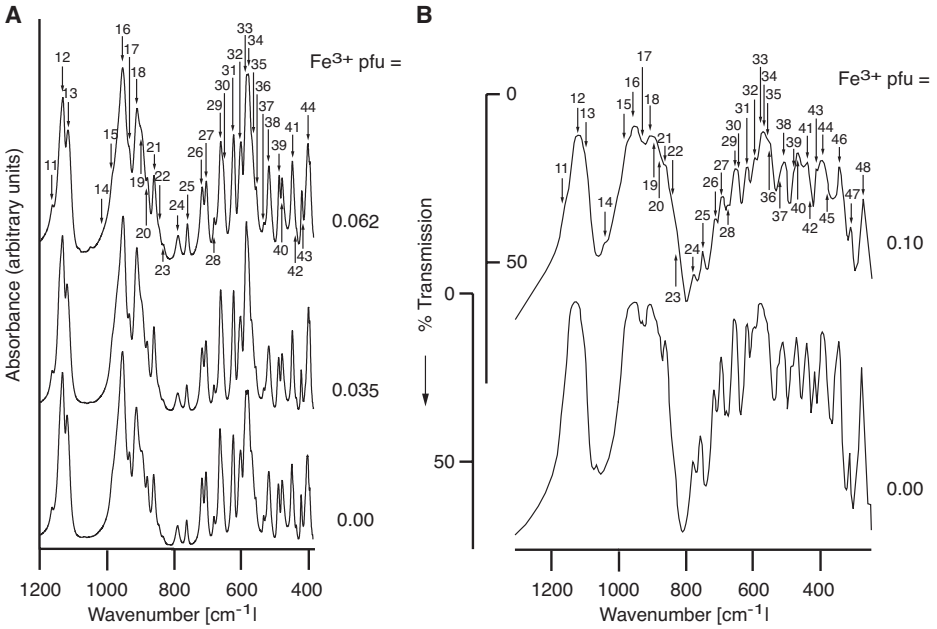

Figure 13. Typical IR spectra of orthorhombic Al-Fe^{3+} solid solutions with different iron contents at (A) −150°C (Liebscher and Gottschalk 2004) and (B) room-temperature (Langer and Raith 1974). Note that the spectra in (A) are displayed in the form of absorbance whereas those in (B) are displayed in the form of transmission. To allow for easier visual comparison between (A) and (B) the spectra in (B) are shown in an unconventional orientation with the transmission increasing downwards. Redrawn and modified after Langer and Raith (1974) and Liebscher and Gottschalk (2004).

epidote minerals are, however, the bands 5 in the spectra of monoclinic epidote minerals, which is missing in the zoisite spectra, and 24 and 25 of the zoisite spectra, which are missing in the spectra of the monoclinic epidote minerals (compare Figs 8 and 13).

Due to the only small compositional variation in zoisite, the positions of the bands show no interpretable shift with the Fe content but rather scatter. Liebscher and Gottschalk (2004) and Liebscher (unpublished data) studied the temperature evolution from −150 to 250°C of the IR spectra of synthetic zoisite below 1200 cm^{-1} (Fig. 14). From those bands they were able to trace over the almost entire temperature range the bands 21 and 26 shift to higher wavenumbers with temperature whereas bands 16, 18, 27, 29, and 41 shift to lower wavenumbers (Fig. 14). Band 27 displays the highest temperature shift. The shift of the bands 29 and 41 is linear over the entire temperature interval whereas that of bands 16, 18, 21, 26, and 27 displays a change in slope at about 50°C (Fig. 14), which is related to the zoisite I–zoisite II phase transition (see below).

Band assignment. As is the case for the monoclinic epidote minerals no rigorous band assignment has yet been performed for the lattice vibrational range of the IR spectra of zoisite. Langer and Raith (1974) assigned the bands 12, 13, 14, 16, 18, 21, 26, and 27 to Si–O valence vibrations of the SiO_4 tetrahedron and/or the Si_2O_7 group. With respect to the Si_2O_7 group, Liebscher and Gottschalk (2004) calculated the theoretical positions of the ν_{as}Si–O–Si and ν_sSi–O–Si vibrations (see Farmer 1974 for terminology) using the dependence of both vibrations on the Si–O–Si bond angle θ from Lazarev (1972) and Farmer (1974) and the values for θ from Liebscher et al. (2002). The ν_{as}Si–O–Si and ν_sSi–O–Si should occur at about

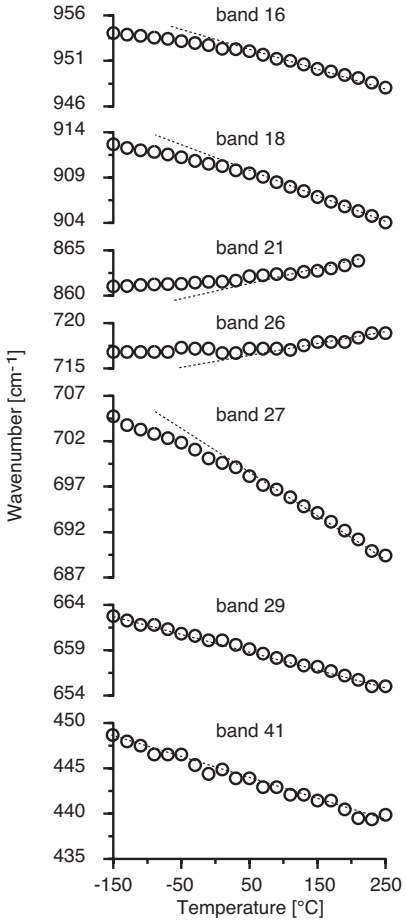

Figure 14. Temperature shift of some IR bands in the lattice vibrational range of synthetic iron free zoisite between −150 and 250°C. Bands that can be tracked over the entire temperature range either shift to higher (bands 21 and 26) or to lower (bands 16, 18, 27, 29, and 41) wavenumber with temperature. The temperature shift of the bands 29 and 41 is linear over the entire temperature interval whereas that of bands 16, 18, 21, 26, and 27 displays a change in slope at about 50°C which relates to the zoisite I–zoisite II phase transition. Dotted lines only visualize these changes in slope. Data are from Liebscher and Gottschalk (2004) and Liebscher (unpublished data).

1,115 and 880 cm^{-1}, respectively (Liebscher and Gottschalk 2004). Therefore either band 12 or 13 can be assigned to ν_{as}Si–O–Si and either band 19 or 20 to ν_{s}Si–O–Si.

By analogy with results from some layer silicates, band 17 at about 930 cm^{-1} was tentatively assigned to an OH bending vibration by Langer and Raith (1974). In a later IR spectroscopy study on a synthetic deuterated zoisite sample Langer and Lattard (1980) abounded this tentative assignment. In the spectrum of the deuterated form they found three additional bands at 815, 730, and 705 cm^{-1} that arise from OD bending vibrations. Applying a ν_{OH}/ν_{OD} factor of 1.34 as a first approximation to account for the isotope effect, the corresponding OH bending vibrations in undeuterated zoisite should occur at 1,090, 975, and 945 cm^{-1} (Langer and Lattard 1980). The proposed band at 1,090 cm^{-1} is most probably obscured by the high intensities of the bands 12 and 13 in the zoisite spectra (see Fig. 13). But consistent with a band at about 1,090 cm^{-1} in the spectrum of undeuterated zoisite, Langer and Lattard (1980) observed a greater width of the bands 12 and 13 in the spectrum of the OH than in the spectrum of the OD form. The proposed OH bending vibration at 975 cm^{-1} coincides with band 15 in the spectra of undeuterated zoisite. Unfortunately, the authors were not able to identify any spectral feature in the spectrum of undeuterated zoisite that could account for the proposed third OH bending vibration at 945 cm^{-1} (Langer and Lattard 1980). As band 27 of the spectrum of undeuterated zoisite is missing in the spectrum of the deuterated form, Langer and Lattard (1980) speculated that this band is due to a fourth OH bending vibration. This interpretation is consistent with two different hydrogen bridges in the zoisite structure (Liebscher et al. 2002). Two hydrogen bridges would result in four theoretical OH bending vibrations in the lattice vibrational range (Langer and Lattard 1980).

Based on the differences between the IR spectra of zoisite and the monoclinic epidote minerals, Langer and Raith (1974) concluded that the zoisite IR bands between 820 to 700 cm^{-1} and 540 to 320 cm^{-1} mainly originate from M-O vibrations within the two different octahedra M1,2 and M3.

OH stretching vibrational region. The OH stretching vibration in zoisite occurs between

3,150 and 3,100 cm^{-1}, at roughly 200 cm^{-1} lower wavenumbers than in the monoclinic Al-Fe^{3+} solid solutions. By means of polarized single crystal IR spectroscopy, Linke (1970) measured the pleochroic scheme of the OH stretching vibration in two zoisite samples that had the optic axial plane parallel (100) (α orientation) and (010) (β orientation), respectively (for a discussion of the α and β orientation see Franz and Liebscher 2004). In both samples he observed a strong pleochroism in thin sections that were cut parallel (100) and (010) with the maximum absorption parallel [001]. Thin sections that were cut parallel (001) did not show any pleochroism (Linke 1970). From his results Linke (1970) concluded that the three dimensional absorption figure of the OH stretching vibration in zoisite, like that in the monoclinic epidote minerals (see above), is an elongated lemniscate that rotates around [001] and that the OH dipole is oriented parallel [001]. This orientation is consistent with an O10–H…O4 hydrogen bridge and confirms the previous findings of Dollase (1968). Linke (1970) also noticed that the three dimensional absorption figure of the OH stretching vibration is identical in the α and β orientation, respectively, and therefore cannot be responsible for the different orientation of the optic axial plane in zoisite.

In their IR spectroscopic study on natural and synthetic zoisite samples of different composition, Langer and Raith (1974) fitted the OH stretching region of the spectra by three bands (bands 2, 5, and 7 in Fig. 15b). They assigned band 5 to the OH stretching vibration and interpreted the bands 2 and 7 as resulting from a coupling of band 5 with lattice vibrations at about 100 cm^{-1}. Contrary, in their study on synthetic Fe free and Fe bearing zoisite Liebscher et al. (2002) fitted the OH stretching region in synthetic Fe free zoisite with four bands (bands 2, 3, 5, and 7; lowermost spectrum in Fig. 15a) and that in Fe bearing zoisite with seven bands (bands 1 to 7; upper two spectra in Fig. 15a). In accordance with Langer and Raith (1974) they assigned band 5 to the OH stretching vibration of the configuration $^{[M1,2]}Al_2$–O10–H…O4–$^{[M1,2]}Al_2{}^{[M3]}Al$. As band 4 is only present in Fe bearing zoisite and the relative intensities of the bands 4 and 5 correlate well with the amounts of Fe^{3+} (band 4) and Al (band 5) in the samples as determined by electron microprobe, Liebscher et al. (2002) assigned band 4 to the OH stretching vibration of the configuration $^{[M1,2]}Al_2$–O10–H…O4–$^{[M1,2]}Al_2{}^{[M3]}Fe^{3+}$. In line with the interpretation of Langer and Raith (1974), the bands 1, 3, 6, and 7 result from a coupling of bands 4 and 5 with lattice vibrations at about 100 cm^{-1}. Because in pure Al-Fe^{3+} zoisite only the above mentioned configurations for the O10–H…O4 hydrogen bridge can occur, band 2 which is present in all spectra can neither be due to this hydrogen bridge nor to the incorporation of Fe^{3+}. By comparing the compositional shift of band 2 with the corresponding X-ray diffraction data, Liebscher et al. (2002) concluded that band 2 arises from the stretching vibration of a second hydrogen bridge of the configuration $^{[M1,2]}Al_2$–O10–H…O2–$^{[M3]}(Al,Fe^{3+})$. This second hydrogen bridge O10–H…O2 was already discussed although not proven by Smith et al. (1987) based on their neutron and X-ray diffraction study. As O10 and the proton both lie on a mirror plane whereas O2 has a general position, the O10–H…O2 hydrogen bridge should be bifurcated between the two symmetrically arranged O2 atoms (Liebscher et al. 2002).

Due to the only small compositional variations within the zoisite solid solutions, the compositional shift of the main OH band 5 is not as clear as in the monoclinic members. Nevertheless, the data indicate a slightly positive correlation between the Fe content and the position of band 5 (Fig. 16). The influence of pressure and temperature on the main OH stretching vibration (band 5) has been studied by Winkler et al. (1989) and Liebscher (unpublished data), respectively. The data of Winkler et al. (1989) for the pressure dependence at room temperature up to 11.6 GPa show a significant linear shift of band 5 to lower wavenumber with increasing pressure (Fig. 17a). With −33.8 cm^{-1}/GPa this shift is markedly more pronounced than in clinozoisite (see above). Taking the bulk modulus for zoisite from Comodi and Zanazzi (1997) of K_0 = 114 GPa, the corresponding Grüneisen parameter for band 5 is $\gamma = -1.22$, about six times smaller than in clinozoisite (Bradbury and Williams 2003; see above). Like in clinozoisite not only a shift of band 5 with pressure is observed in

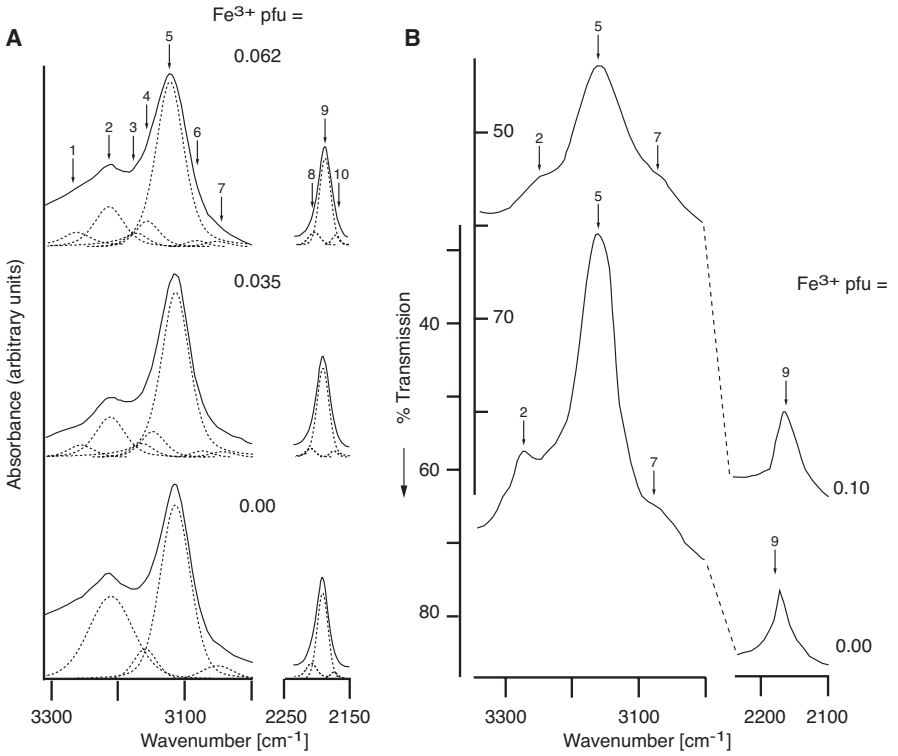

Figure 15. Typical IR spectra of orthorhombic Al-Fe^{3+} solid solutions in the region of the OH stretching vibration and between 2250 and 2100 cm^{-1} at (A) −150°C (Liebscher et al. 2002) and (B) room-temperature (Langer and Raith 1974). Note that the spectra are displayed in the form of absorbance in (A) and in the form of transmission in (B). The spectra in (B) are shown with the transmission increasing downwards and are to scale. In the orthorhombic Al-Fe^{3+} solid solutions the OH stretching vibration is characterized by a maximum between about 3200 and 3100 cm^{-1} (band 5; configuration $^{[M1,2]}Al_2$-O10-H…O4-$^{[M1,2]}Al_2{}^{[M3]}Al$). Band 2 arises from a second hydrogen bridge O10–H…O2. Band 4 is only present in iron bearing zoisite and arises from the configuration $^{[M1,2]}Al_2$-O10-H…O4-$^{[M1,2]}Al_2{}^{[M3]}Fe^{3+}$. Redrawn and modified after Langer and Raith (1974) and Liebscher et al. (2002).

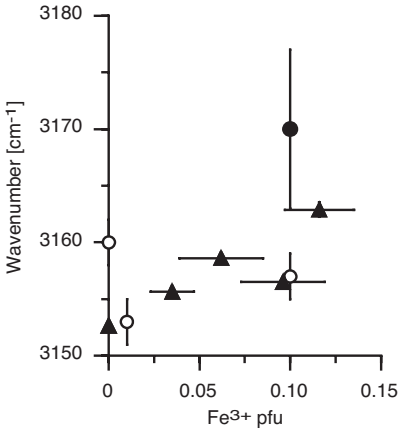

Figure 16. Compositional shift of the zoisite IR band 5. The data scatter but indicate a positive compositional shift of band 5. Data sources are as follows: ○ = Langer and Raith (1974), ● = Winkler et al. (1989), and ▲ = Liebscher et al. (2002).

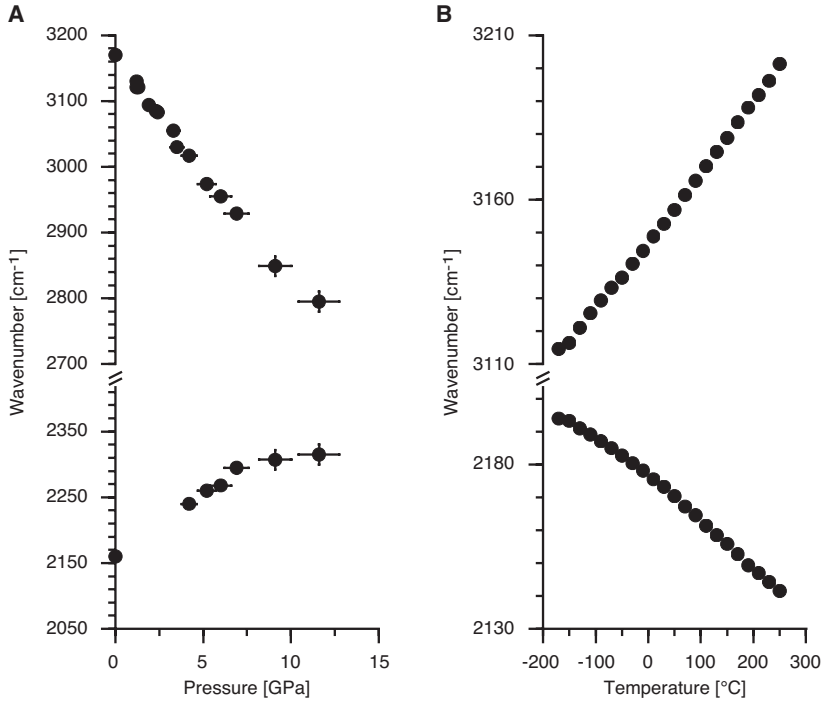

Figure 17. Pressure (A) and temperature (B) shifts of the zoisite IR bands 5 and 9. Band 5 shifts linearly to lower wavenumber with pressure and to higher wavenumber with temperature whereas band 9 displays the opposite behavior.

zoisite, but also a significant broadening of band 5 (Winkler et al. 1989). The half width of band 5 increases by about 27 cm^{-1}/GPa, about three-times the value observed in clinozoisite (Bradbury and Williams 2003). Based on their model derived for clinozoisite, Bradbury and Williams (2003) speculated that the dramatic shift and broadening of the zoisite OH stretching vibration may be related to the initially shorter hydrogen bond in zoisite and a correspondingly closer initial approach of the two potential minima (see Fig. 12). The temperature shift to higher wavenumber of band 5 is linear with 0.21 cm^{-1}/°C over the entire investigated temperature range from −170 to 250°C (Fig. 17b; Liebscher unpublished data).

Band 9 at 2,300 to 2,100 cm^{-1}. The band 9 between 2,300 and 2,100 cm^{-1} is a unique feature of the IR spectrum of zoisite compared to the spectra of the monoclinic epidote minerals. Compared to the main OH stretching vibration (band 5) the intensity of band 9 is very low (Fig. 15b; note that the spectra in Fig. 15a are not to scale). Contrary to band 5, which shifts to higher wavenumber with increasing Fe content, band 9 shifts to lower wavenumber (Liebscher et al. 2002). Langer and Raith (1974) assigned band 9 to a second OH stretching vibration that arises from a second hydrogen bridge in the zoisite structure. Band 9 has a notable low energy for an OH stretching vibration, and Langer and Raith (1974) calculated an O–O distance for the proposed underlying second hydrogen bridge of only 2.56 Å. Such a short O–O distance exists only between oxygen atoms that form edges of the coordination polyhedra and Langer and Raith (1974) therefore concluded, "it is uncertain which oxygen atoms are involved in the short bridge." The spectrum of a deuterated zoisite recorded by Langer and Lattard (1980) shows a shift of band 9 to a lower wavenumber by a factor of 1.35

and thus proved band 9 to arise from some proton related vibration. The interpretation of band 9 as an OH stretching vibration by Langer and Raith (1974) was later questioned by Winkler et al. (1989) based on the pressure shift of band 9 and polarized single crystal IR data. Contrary to band 5 that shifts to lower wavenumber with increasing pressure, band 9 shifts to higher wavenumber on compression (Fig. 17a) consistent with an OH bending vibration and Winkler et al. (1989) therefore assigned band 9 to the first overtone of the in-plane bending vibration of the O10–H…O4 hydrogen bridge. Nevertheless, as the first overtone of the OH bending vibration should occur at a lower energy of about 2,000 to 1,950 cm^{-1} (Langer and Raith 1974), the interpretation of Winkler et al. (1989) could not explain the comparable high energy of band 9. Consistent with the interpretation of band 9 as a bending vibration, Liebscher et al. (2002) and Liebscher (unpublished data) found a shift to lower wavenumber of band 9 with temperature (Fig. 17b). As there is also evidence for a second hydrogen bridge O10–H…O2 that must be bifurcated (band 2; see above), band 9 is interpreted as the first overtone of the in-plane bending vibration of the O10–H…O2 hydrogen bridge, and the bifurcated nature of this hydrogen bridge well explains the comparable high energy of band 9 (Liebscher et al. 2002).

Phase transition in zoisite. Brunsmann (2000), Liebscher et al. (2002), and Liebscher and Gottschalk (2004) used IR spectroscopy to study the isosymmetric displacive phase transition in zoisite (see Franz and Liebscher 2004). In good accordance with the results from X-ray diffraction the IR spectra of the studied synthetic zoisite samples show discontinuities in their compositional shift at about 0.05 Fe^{3+} pfu. To study the temperature dependence of the phase transition, Liebscher and Gottschalk (2004) performed a temperature dependent IR spectroscopic study between −150 and 170°C. Whereas some of the IR bands show a linear shift with temperature over the entire temperature interval, others show a smaller linear positional shift with temperature at low than at high temperature (see Fig. 14). This change in slope has been interpreted as the transition from zoisite I to zoisite II. To account for strongly overlapping bands especially at higher temperature that may place some doubt on the exact determination of the band positions, the authors analyzed the spectra in the spectral range 1,050 to 820 cm^{-1} (bands 14 to 23) by means of autocorrelation (Salje et al. 2000). Like the band positions, the autocorrelation analyses show a different low and high temperature evolution of the spectra in all samples (Fig. 18a). This different temperature evolution is best displayed by

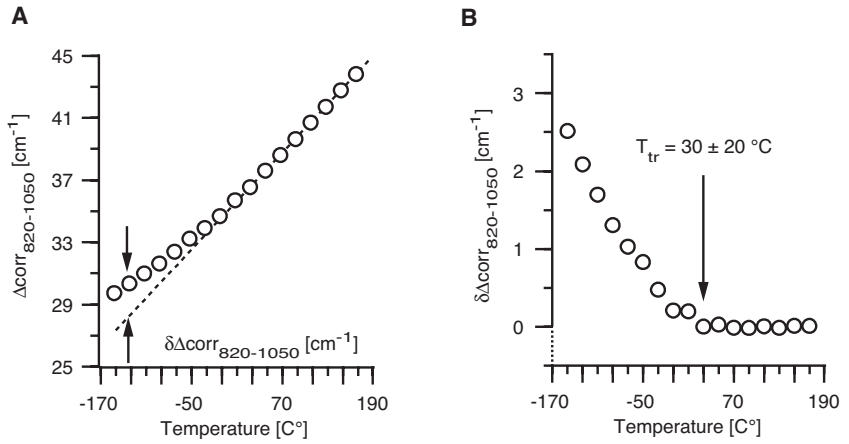

Figure 18. (A) Autocorrelation analysis of the spectral range 1050 to 820 cm^{-1} and (B) the corresponding excess line width parameter $\delta\Delta_{corr}$ for an iron free zoisite. The data show a different low and high temperature evolution of the spectrum. The change from the low to the high temperature evolution marks the transition from zoisite I to zoisite II (redrawn after Liebscher and Gottschalk 2004).

the excess line width parameter $\delta\Delta_{corr}$ (Salje et al. 2000) that clearly shows the transition from zoisite I to zoisite II (Fig. 18b). The data of Liebscher and Gottschalk (2004) indicate that the transition temperature T_{tr} correlates negatively with the Fe content and a tentative linear fit to their data yields $T_{tr} = 57 - 1223\ X_{Fe}$ [°C].

MÖSSBAUER SPECTROSCOPY

So far, studies on epidote minerals are restricted to the monoclinic members and to ^{57}Fe-Mössbauer spectroscopy. De Coster et al. (1963) published the first Mössbauer spectrum of an epidote of unspecified composition and origin. Later, Marfunin et al. (1967) reported the 80 and 300 K spectra of an epidote of unspecified composition and Bancroft et al. (1967) studied the spectra of two epidotes with $X_{Ep} = 0.84$ and 0.87, respectively, and one piemontite with 0.63 Mn^{3+} and 0.33 Fe^{3+} pfu. Dollase (1971) published the first Mössbauer spectrum of allanite and later studied systematically the spectra of and the Fe distribution in 33 samples of natural and synthetic epidote minerals including Al-Fe^{3+} solid solutions with $X_{Ep} = 0.36$ to 1.00, piemontites, allanites, and oxyallanites (Dollase 1973). Temperature dependent spectra down to 2 K were recorded by Pollak and Bruyneel (1975) and Paesano et al. (1983). Whereas these early studies focused their work primarily on the determination of the valence state of Fe and the Fe site assignment, Bird et al. (1988) and Patrier et al. (1991) used ^{57}Fe-Mössbauer spectroscopy to study the equilibrium or nonequilibrium compositional order/disorder in natural epidote samples as a function of the physicochemical conditions during epidote formation. Fehr and Heuss-Aßbichler (1997) and Heuss-Aßbichler (2000) later extended these studies and determined the intracrystalline ordering of Al and Fe^{3+} in Al-Fe^{3+} solid solutions by means of ^{57}Fe-Mössbauer spectroscopy on natural heat treated samples with $X_{Ep} = 0.39$ to 0.98. A theoretical treatment of the Mössbauer spectra of Fe rich Al-Fe^{3+} solid solutions by molecular orbital calculations was then presented by Grodzicki et al. (2001). The results of the different studies in terms of the fitted Mössbauer parameters are summarized in Table 1.

Mössbauer spectra of the different epidote minerals

Monoclinic Al-Fe^{3+} solid solutions. In the monoclinic Al-Fe^{3+} solid solutions Fe is almost exclusively in the ferric state and shows a very strong affinity for the M3 site compared to the M1 and M2 sites (see Franz and Liebscher 2004). Their Mössbauer spectra are therefore in most cases simple (Dollase 1973). All spectra of the monoclinic Al-Fe^{3+} solid solutions are characterized by one very prominent doublet (Fig. 19a,b) and the reported Mössbauer parameters for this doublet are consistent between the different studies. Its isomer shift (IS) relative to α-Fe ranges from 0.31 to 0.44 mm/sec (note that all isomer shift data presented in this review were recalculated relative to α-Fe to allow for comparison) and the quadrupole splitting (QS) is 1.89 to 2.096 mm/sec (Fig. 20a). This isomer shift is characteristic for Fe^{3+} in octahedral coordination whereas the quadrupole splitting is one of the largest observed for a high-spin Fe^{3+} compound and points to a strongly distorted site (Bancroft et al. 1967; the high-spin electronic state of Fe^{3+} in epidote group minerals was deduced by Burns and Strens 1967 based on magnetic susceptibility measurements). Consequently, this doublet has been assigned to Fe^{3+} in M3 by all studies (Fig. 19a,b; for a splitting of this doublet into two components M3 and M3′ in Al-Fe^{3+} solid solutions with $X_{Ep} < 0.7$ see below).

Although the earliest studies fitted the recorded epidote spectra exclusively with one doublet for Fe^{3+} in M3 (De Coster et al. 1963; Bancroft et al. 1967; Marfunin et al. 1967), later and more detailed studies clearly show doublets of minor intensity in addition to that for Fe^{3+} in M3 in most of the studied spectra of monoclinic Al-Fe^{3+} solid solutions. It should be noted that of the early studies mentioned at least the epidote spectrum reported by Marfunin et al. (1967) suggests a second doublet that was not fitted by the authors. The Mössbauer parameters for these additional minor doublets determine three distinct groups (Fig. 20a). In addition to

Table 1. Isomer shift IS [mm/sec] relative to α-iron, quadrupole splitting QS [mm/sec], and full width at half maximum FWHM [mm/sec] for the different doublets fitted to the spectra of epidote minerals

	Al-Fe^{3+} solid solutions	Piemontite	Allanite	Ferriallanite	Oxyallanite
Fe^{3+} in M1					
IS	0.22–0.36[1, 3, 7]		0.29–0.29[2]	0.36[6]	0.34–0.36[1]
QS	1.46–1.67[1, 3, 7]		1.01–1.36[2, 4, 11]	1.78[6]	1.84–1.91[1]
FWHM	0.23–0.51[1, 3, 7]		0.40–0.74[2, 4]		0.41–0.45[1]
Fe^{3+} in M2 (as recommended in this review, see text)					
IS	0.31–0.37[5, 8]	0.25–0.33[1]		0.334[6]	
QS	0.80–1.0[5, 8]	0.83–1.13[1]		0.85[6]	
FWHM	0.40–0.50[5, 8]	0.40–0.52[1]			
Fe^{3+} in M3					
IS	0.31–0.44 [1, 3, 5, 7, 8, 9, 10, 12]	0.34–0.37 [1, 10]	0.37–0.55 [1, 2, 11]		0.35–0.36 [1]
QS	1.89–2.10 [1, 3, 5, 7, 8, 9, 10, 12]	2.0–2.02 [1, 10]	1.61–2.00 [1, 2, 4, 11]		2.26–2.31 [1]
FWHM	0.25–0.49 [1, 3, 5, 7, 8, 9, 10, 12]	0.40–0.52 [1, 10]	0.30–0.58 [1, 2, 4, 11]		0.41–0.45 [1]
Fe^{3+} in M3´					
IS	0.24–0.36[7]				
QS	1.99–2.32[7]				
FWHM	0.22–0.35[7]				
Fe^{3+} in unspecified site					
IS			0.35–0.39[1]	1.07[6]	
QS			1.87–1.97[1]	1.62[6]	
FWHM			0.37–0.47[1]		
Fe^{2+} in M3					
IS	1.09–1.40[7]		1.07–1.08[1, 2, 11]	1.07[6]	
QS	1.78–2.42[7]		1.63–1.83[1, 2, 4, 11]	1.62[6]	
FWHM	0.26–0.73[7]		0.35–0.58[1, 2, 4, 11]		
Fe^{2+} in M1					
IS			1.24–1.24[2, 11]		
QS			1.93–2.07[2, 4, 11]		
FWHM			0.40–0.58[2, 4, 11]		
Fe^{2+} in unspecified site					
IS	1.07–1.30[1, 8]				1.09–1.14[1]
QS	1.8–2.28[1, 8]		1.87–2.14[1]		1.62–1.72[1]
FWHM	0.32–0.44[1, 8]		0.35–0.42[1]		0.34–0.60[1]

Note. Small numbers in parentheses refer to following sources: [1] Dollase (1973); [2] Dollase (1971); [3] Bird et al. (1988); [4] Mingsheng and Daoyuan (1986) and Mingsheng and Dien (1987); [5] Artioli et al. (1995); [6] Kartashov et al. (2002); [7] Fehr and Heuss-Aßbichler (1997) and Heuss-Aßbichler (2000); [8] Patrier et al. (1991); [9] De Coster et al. (1963); [10] Bancroft et al. (1967); [11] Lipka et al. (1995); [12] Marfunin et al. (1967)

the doublet for Fe^{3+} in M3, Dollase (1973), Bird et al. (1988), and Fehr and Heuss-Aßbichler (1997) fitted some of their spectra with a second doublet that has IS = 0.217 to 0.355 mm/sec and QS = 1.455 to 1.666 mm/sec (Fig. 20a). The range in the isomer shift of this second doublet is comparable to the main doublet for Fe^{3+} in M3 but its quadrupole splitting is smaller and suggests a slightly less distorted site (Bancroft et al. 1967). The authors therefore assigned this doublet to Fe^{3+} in M1 (Fig. 19a). Contrary to the aforementioned authors, Patrier et al. (1991) and Artioli et al. (1995) evaluated most of their spectra with a second doublet that has a comparable isomer shift (0.31 to 0.37 mm/sec) but a notable smaller QS of only 0.8 to 1.0 mm/sec (Figs19b, 20a). Notwithstanding this significant difference in QS, Patrier et al. (1991) and Artioli et al. (1995) also assigned the second doublet to Fe^{3+} in M1. A comparison with the spectrum of a ferriallanite (Fig. 19e, Kartashov et al. 2002; see below) indicates that this assignment by Patrier et al. (1991) and Artioli et al. (1995) might be incorrect. One of the doublets in the spectrum of the ferriallanite has IS = 0.334 mm/sec and QS = 0.85 mm/sec. These values are identical to those found by Patrier et al. (1991) and Artioli et al. (1995) for the second, low intensity doublet. As the doublet in the ferriallanite spectrum must be assigned to Fe^{3+} in M2 (Kartashov et al. 2002; see below) the second doublet of Patrier et al. (1991) and Artioli et al. (1995) probably also arises from Fe^{3+} in M2. This potentially incorrect assignment of the second doublet to Fe^{3+} in M1 by Patrier et al. (1991) would also explain the erroneously high disorder these authors claimed for the intracrystalline partitioning of Al and Fe^{3+} between M3 and M1 as the authors actually studied the partitioning of Al and Fe^{3+} between M3 and M2.

Beside the doublets that can be assigned to Fe^{3+} based on the isomer shift, Dollase (1973), Patrier et al. (1991), and Fehr and Heuss-Aßbichler (1997) found evidence in some of the recorded spectra for small amounts of Fe^{2+} in the studied samples (Fig. 19a,b). These spectra show a very low intensity doublet with IS = 1.065 to 1.295 mm/sec and QS = 1.8 to 2.28 mm/sec (Fig. 20a). This isomer shift is characteristic for Fe^{2+} in octahedral coordination (Bancroft et al. 1967). Unfortunately, due to the low intensity of this doublet in the studied spectra, neither Dollase (1973) nor Patrier et al. (1991) were able to assign it unequivocally to Fe^{2+} in a specific site. Dollase (1973) even discussed the possibility that this doublet may arise from some undetected Fe bearing impurity phases. In contrast, Fehr and Heuss-Aßbichler (1997) assigned this doublet to Fe^{2+} in the largest and most distorted octahedron M3.

Each of the three doublets assigned to Fe^{3+} has very homogeneous Mössbauer parameters. The range in the isomer shift is identical for all three doublets and shows no dependence on composition. Likewise, the quadrupole splitting although of a characteristic value for each doublet is independent on composition (Fig. 21). This indicates that changes in the distortion of the individual octahedra with increasing Fe content are too small to be resolved. It is also evident from Figure 21 that the doublet for Fe^{3+} in M3 appears throughout the entire compositional range and that it is the only doublet present in the spectra of solid solutions with $X_{Ep} < 0.7$. This is consistent with the structural and optical data for the monoclinic Al-Fe^{3+} solid solution series that also indicate exclusive incorporation of Fe^{3+} in M3 for Fe contents below about $X_{Ep} = 0.7$ (see Franz and Liebscher 2004). The other two doublets for Fe^{3+} in M1 and, potentially, M2 are only found in the spectra of Al-Fe^{3+} solid solutions with $X_{Ep} > 0.7$. For these high Fe contents, the structural data as well as detailed crystal chemical studies (e.g., Giuli et al. 1999) also provide good evidence for incorporation of appreciable amounts of Fe in M1 and, under specific conditions, of small but notable amounts of Fe in M2 (see Franz and Liebscher 2004). In this context it should be noted that none of the Mössbauer studies has yet resolved both minor doublets for Fe^{3+} in M1 and M2 in one and the same spectrum although the data of Giuli et al. (1999) strongly suggest that Fe substitutes simultaneously in M1 and M2. This inconsistency might be partly due to the low intensity of the two doublets in question that makes their fitting very difficult but most probably reflects the pre-assumption of most studies that the M2 position is entirely filled with Al, which let the authors not to search for a third doublet.

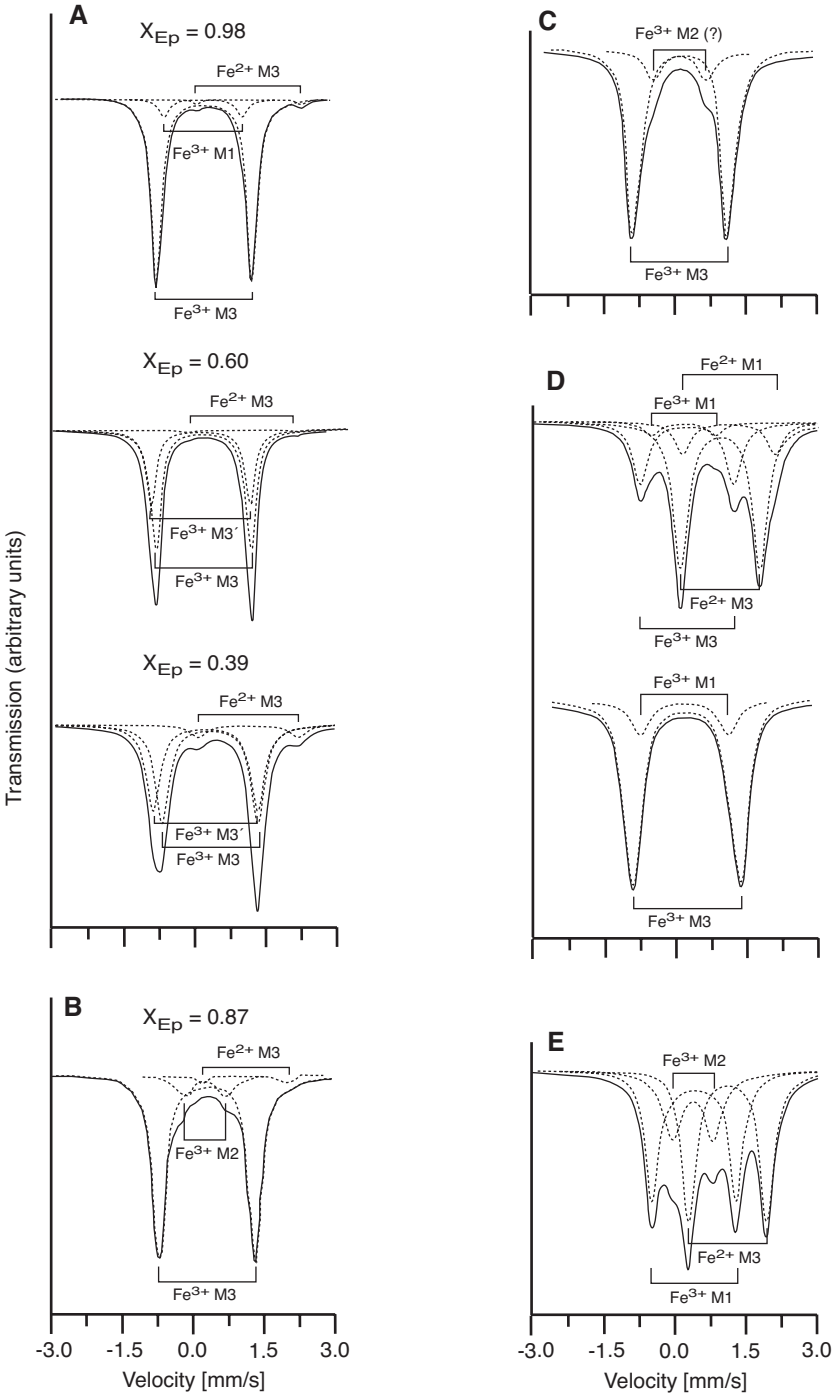

Figure 19. *caption at top of facing page*

Figure 19 (*on facing page*). Typical room-temperature Mössbauer spectra of (A) and (B) Al-Fe^{3+} solid solutions, (C) piemontite, (D) allanite and oxyallanite, and (E) ferriallanite. For the assignment of the two doublets to Fe^{3+} in M3 and M3´ in the two lower spectra of (A) see text. The low intensity Fe^{3+} doublets in (B) and (C) are assigned to M2 by comparison with the ferriallanite spectrum (E). In the original papers, these doublets are assigned to Fe^{3+} in M1. The two spectra in (D) represent one and the same allanite sample before (upper spectrum) and after (lower spectrum) heat treatment and complete oxidation. Redrawn and modified after (A) Fehr and Heuss-Aßbichler (1997) and Heuss-Aßbichler (2000), (B) Patrier et al. (1991), (C) and (D) Dollase (1973), and (E) Kartashov et al. (2002).

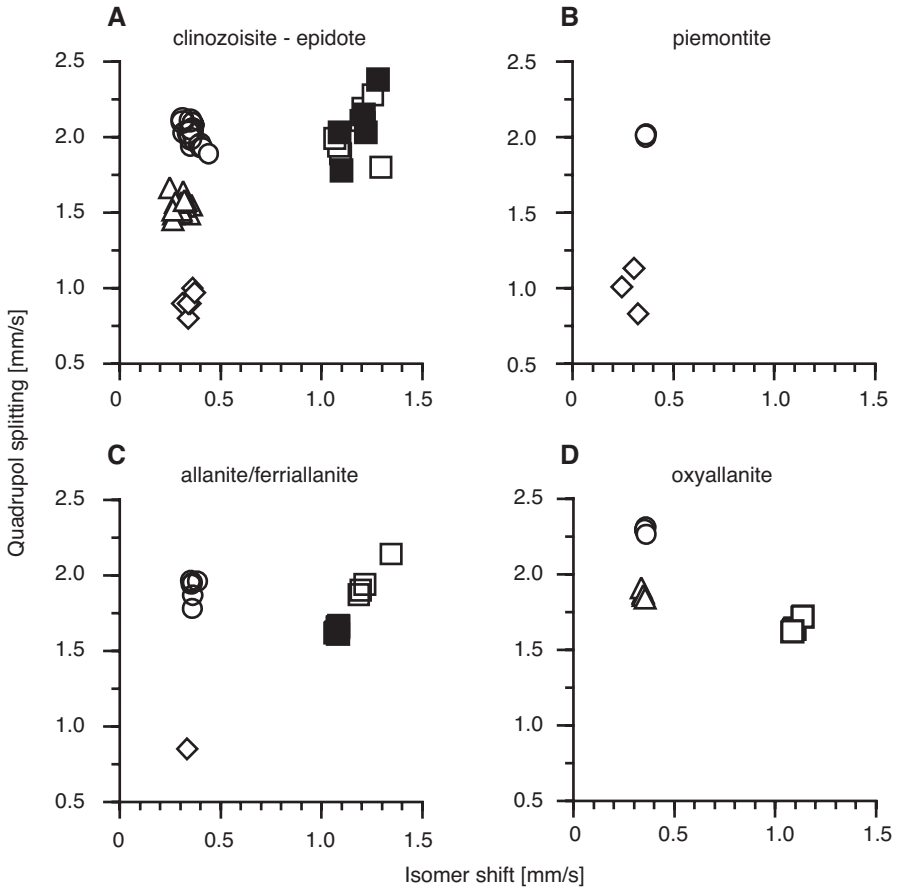

Figure 20. Quadrupole splitting and isomer shift (recalculated relative to α-iron) of the different doublets fitted to the Mössbauer spectra of (A) Al-Fe^{3+} solid solution, (B) piemontite, (C) allanite and ferriallanite, and (D) oxyalllanite. ○ = Fe^{3+} in M3, △ = Fe^{3+} in M1, ◇ = Fe^{3+} in M2 (as recommended in this review, the original papers assigned these doublets also to Fe^{3+} in M1, see text), ■ = Fe^{2+} in M3, □ = Fe^{2+} in unspecified site. Data from Bancroft et al. (1967), Dollase (1971, 1973), Bird et al. (1988), Patrier et al. (1991), Artioli et al. (1995), Fehr and Heuss-Aßbichler (1997), Heuss-Aßbichler (2000), and Kartashov et al. (2002).

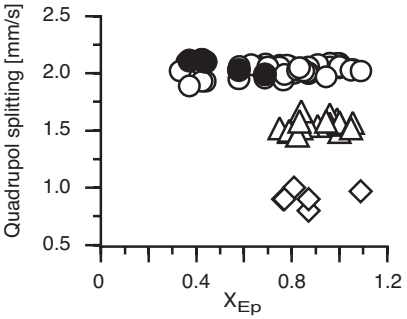

Figure 21. Quadrupole splitting of Fe^{3+} in the different octahedral sites in Al-Fe^{3+} solid solutions as a function of composition. ○,● = Fe^{3+} in M3 (● refer to Fe^{3+} in M3′, see text), △ = Fe^{3+} in M1, ◇ = Fe^{3+} in M2 (as recommended in this review, the original papers assigned these doublets also to Fe^{3+} in M1, see text). Data from Bancroft et al. (1967), Dollase (1973), Bird et al. (1988), Patrier et al. (1991), Artioli et al. (1995), Fehr and Heuss-Aßbichler (1997), and Heuss-Aßbichler (2000).

Temperature dependent Mössbauer spectra are recorded by Pollak and Bruyneel (1975) for an epidote of unspecified composition between 300 and 4.2 K and by Paesano et al. (1983) for an epidote with $X_{Ep} = 0.96$ between 300 and 2 K (Fig. 22a). Down to 100 K the spectra recorded by Pollak and Bruyneel (1975) show no significant changes. All spectra could be fitted with one doublet with Mössbauer parameters typical for Fe^{3+} in M3 (Fig. 22b). Contrary, the spectrum recorded at 4.2 K display three superposed symmetric doublets that were tentatively assigned to Fe^{3+} in M3, M2, and M1 by Pollak and Bruyneel (1975). Whereas the doublet assigned to Fe^{3+} in M3 shows the typical Mössbauer parameters, the two doublets assigned to Fe^{3+} in M2 and M1, respectively, are characterized by a notable small quadrupole splitting and isomer shift (Fig. 22c). Unfortunately, Pollak and Bruyneel (1975) did not find a conclusive explanation for the appearance of the two additional doublets in the 4.2 K spectrum. Paesano et al. (1983) recorded Mössbauer spectra down to 2 K with special emphasis given to the low temperature region. Down to 77 K the spectra show a well-defined and symmetric doublet that can be attributed to Fe^{3+} in M3 based on the Mössbauer parameters (Fig. 22b; Paesano et al. 1983). Below 10 K the character of the spectra change, the doublet for Fe^{3+} in M3 becomes increasingly asymmetric and below 4 K a well-defined magnetic hyperfine structure appears (Fig. 22a). But throughout the entire investigated temperature range, Paesano et al. (1983) did not find any evidence for Fe^{3+} in another site than M3 (Fig. 22b,c). From the results of their fits to the low temperature spectra, they concluded that the magnetic hyperfine structure observed below 4 K results from "a freezing of the paramagnetic moment on Fe^{3+}." As the spectra recorded at 3 and 2 K show a constant hyperfine field, no magnetic transition has occurred and they speculated that the additional structures observed by Pollak and Bruyneel (1975) in the 4.2 K spectrum arise from a paramagnetic hyperfine structure instead of Fe^{3+} in the M1 and M2 sites.

Grodzicki et al. (2001) carried out cluster molecular orbital calculations in local spin density approximation to understand the observed quadrupole splittings of Fe^{3+} in M3 and M1 and of Fe^{2+} in M3. To obtain Mössbauer parameters that are consistent with the experimental results, the chosen clusters have to be rather large. Beside the first coordination shell, they must at least include the coordination spheres of the oxygen atoms bound to Fe. Based on clusters fulfilling these requirements, the authors calculated quadrupole splittings of −1.89 to −2.09 mm/sec for Fe^{3+} in M3 (for Al-Fe^{3+} solid solutions with X_{Ep} = 0.60 to 0.89 and an allanite), −1.30 mm/sec for Fe^{3+} in M1 (for an Al-Fe^{3+} solid solution with $X_{Ep} = 0.76$) and +2.03 mm/sec for Fe^{2+} in M3. These values quantitatively agree with the experimentally determined ones (see Table MS 1). The large quadrupole splitting calculated and observed for Fe^{3+} in M3 is due to the strong tetragonal compression of this site whereas the smaller quadrupole splitting of Fe^{3+} in M1 reflects the smaller tetragonal compression of M1 (Grodzicki et al. 2001). The strong tetragonal compression of M3 is also responsible for the observed and calculated quadrupole splitting of Fe^{2+} in M3 (~2.0 mm/sec), which is considerable smaller than the 2.60 to 3.60 mm/sec range commonly observed for the quadrupole splitting of Fe^{2+} in minerals (Grodzicki et al. 2001).

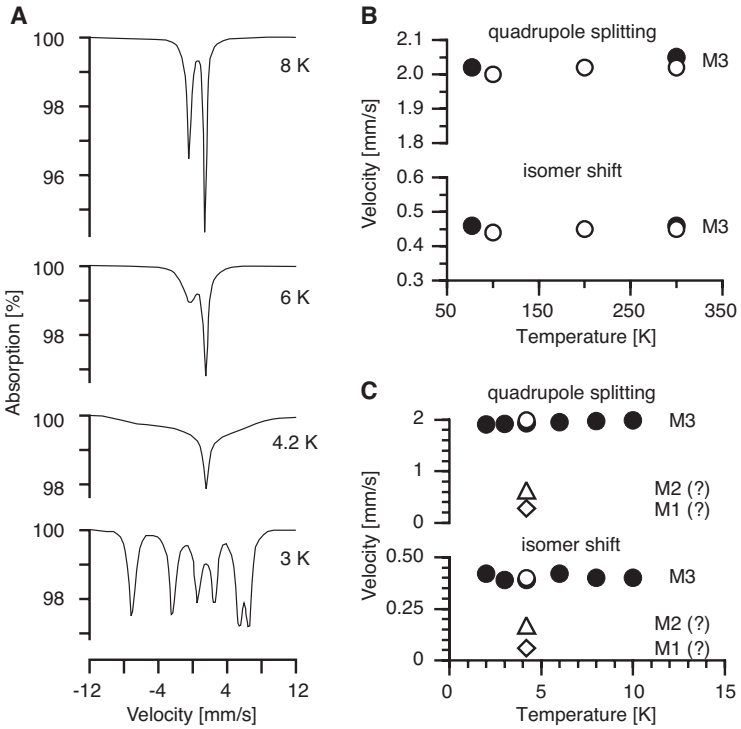

Figure 22. Evolution of the Mössbauer spectra of Al-Fe^{3+} solid solutions with decreasing temperature. (A) Low-temperature Mössbauer spectra of an epidote with $X_{Ep} = 0.96$ (redrawn and modified after Paesano et al. 1983). (B) and (C) Temperature dependence of quadrupole splitting and isomer shift (relative to α-iron) of Fe^{3+} in Al-Fe^{3+} solid solutions between 300 and 50 K (B) and between 10 and 2 K (C). Data from Pollak and Bruyneel (1975; open symbols) and Paesano et al. (1983; filled symbols). Pollak and Bruyneel (1975) fitted their 4.2 K spectrum with three doublets and assigned them to Fe^{3+} in M3, M2 (diamond), and M1 (triangle). The Mössbauer parameter for Fe^{3+} in M3 (filled and open circles) are constant over the entire temperature range.

Piemontite. Like in the monoclinic Al-Fe^{3+} solid solutions, Fe is predominantly ferric in the piemontite solid solutions. Only in REE bearing piemontite samples, Fe^{2+} might occur in appreciable amounts. The Mössbauer spectra of piemontite solid solutions therefore closely resemble those of the Al-Fe^{3+} solid solutions (Fig. 19a–c). Bancroft et al. (1967) studied a piemontite with 0.332 Fe^{3+} pfu and 0.625 Mn^{3+} pfu and evaluated it with only one doublet with IS = 0.34 mm/sec and QS = 2.02 mm/sec. Later, Dollase (1973) analyzed the spectra of three piemontite samples with 0.12 to 0.33 Fe^{3+} pfu and 0.72 to 0.86 Mn^{3+} pfu. All three spectra are consistent and in contrast to the results of Bancroft et al. (1967) had to be evaluated by two doublets (Fig. 19c). The main doublet has an isomer shift of 0.362 to 0.365 mm/sec and a quadrupole splitting of 2.0 to 2.02 mm/sec. The second doublet has a much smaller intensity (Fig. 19c), a slightly smaller isomer shift (0.245 to 0.325 mm/sec) and a significantly smaller quadrupole splitting (0.83 to 1.13 mm/sec; Fig. 20b). By analogy with the results from the Al-Fe^{3+} solid solution series, the main doublet can be assigned to Fe^{3+} in M3 whereas the second doublet may arise from Fe^{3+} in M2 (Fig. 19c).

Allanite, oxyallanite, and ferriallanite. In contrast to the Al-Fe^{3+} solid solutions and to piemontite, in which the overwhelming majority of the Fe is normally ferric, it is generally

present as both ferric and ferrous in allanite with Fe^{2+} being the major component (see Gieré and Sorensen 2004). The ferric and ferrous Fe might be distributed over the different octahedral sites and the Mössbauer spectra of allanite are therefore more complicated and often only poorly resolved and ambiguous (Dollase 1973). Dollase (1971) published the first Mössbauer spectrum of an allanite with Fe_{tot} = 1.2 pfu and also provided a first preliminary interpretation of its spectral properties. Later, he studied the Mössbauer spectra of this and three more allanite samples in greater detail and, based on the changes of the spectral properties, analyzed the effects of oxidation and reduction on allanite (Dollase 1973). The Mössbauer spectrum of a partly metamict allanite was presented by Mingsheng and Daoyuan (1986) and Mingsheng and Dien (1987). More recently, Lipka et al. (1995) performed a Mössbauer spectroscopic study on three allanite samples and Kartashov et al. (2002) reported the Mössbauer spectrum of a ferriallanite.

The spectra of allanite are typically evaluated with three or four doublets (Fig. 19d upper spectrum). Based on their isomer shifts these doublets can be confidentially assigned to either ferrous or ferric Fe (Fig. 20c). The main Fe^{2+} doublet that normally displays the highest intensity of all doublets has very consistent Mössbauer parameters throughout the different studies. Its IS ranges from 1.068 to 1.083 mm/sec with a QS of 1.660 to 1.666 mm/sec (Fig. 20c). This doublet is generally assigned to Fe^{2+} in M3. If present, the second Fe^{2+} doublet has a much lower intensity and is therefore only poorly constrained with respect to its peak location. Consequently, its Mössbauer parameters show a greater scatter and range from 1.185 to 1.345 mm/sec (IS) and 1.87 to 2.14 mm/sec (QS) (Fig. 20c). Dollase (1971), Mingsheng and Daoyuan (1986), Mingsheng and Dien (1987), and Lipka et al. (1995) assigned this second doublet to Fe^{2+} in M1 whereas Dollase (1973) claimed, "no unequivocal assignment seems possible with the data at hand." But as the Mössbauer spectra of the oxidized allanite samples (Dollase 1973; see below) exclusively show Fe^{3+} in M3 and M1 and because it can be assumed that no significant Fe diffusion occurred during the oxidization procedure it is reasonable to assume that Fe^{2+} in the unoxidized allanite samples is also restricted to M3 and M1.

Beside the doublets for ferrous Fe, the Mössbauer spectra of allanite typically show one or two doublets that can be assigned to ferric Fe. Dollase (1971), Mingsheng and Daoyuan (1986), Mingsheng and Dien (1987), and Lipka et al. (1995) evaluated their spectra with two doublets for Fe^{3+} and assigned them to M3 and M1, respectively (Fig. 19d upper spectrum). The corresponding Mössbauer parameters are 0.37 to 0.55 mm/sec (IS) and 1.61 to 1.97 mm/sec (QS) for Fe^{3+} in M3 and 0.22 to 0.29 mm/sec (IS) and 1.33 to 1.36 mm/sec (QS) for Fe^{3+} in M1. Contrary, Dollase (1973) failed in fitting two ferric doublets to the studied allanite spectra and reports only a single ferric doublet without specific site assignment. The parameters of this doublet are IS = 0.351 to 0.385 mm/sec and QS = 1.78 to 1.965 mm/sec. But as this quadrupole splitting is substantially smaller than that attributed to Fe^{3+} in M3 in the Al-Fe^{3+} solid solutions, there is good indication that the single ferric doublet actually represents two separate but strongly overlapping doublets (Dollase 1973).

To study the effect of oxidation on allanite, Dollase (1973) heat-treated two of the studied allanite samples in air at 370 to 700°C for 46 to 163 hours and analyzed the evolution of the ferric/ferrous ratios by means of Mössbauer spectroscopy (for a more general and thorough discussion of oxyallanite see Gieré and Sorensen 2004). Up to T = 400°C he did not observe any change in the ferrous/ferric ratio (Fig. 23). For T > 400°C the intensities of the doublets assigned to Fe^{3+} continuously increase with increasing temperature whereas those assigned to Fe^{2+} decrease. In one sample this results in an increase of the calculated $X_{Fe3+} = Fe^{3+}/Fe_{tot}$ from 0.32 in the untreated sample to 0.88 in the sample that was heat-treated at 680°C and in almost complete oxidation at 700°C (Fig. 23). The corresponding Mössbauer spectrum of the fully oxidized allanite exhibits only two doublets that can be confidentially assigned to Fe^{3+} in M3 and M1 (Fig. 19d lower spectrum). As none of the spectra of the partly to fully oxidized allanite

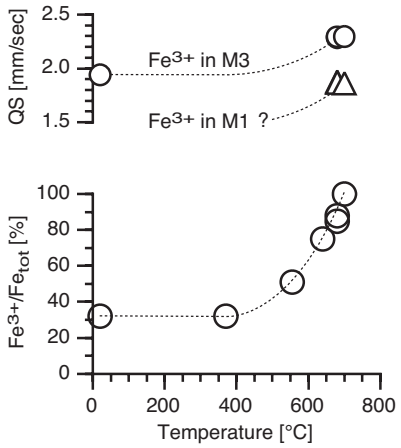

Figure 23. Oxidation of Fe^{2+} to Fe^{3+} in natural allanite as determined by Mössbauer spectroscopy. Up to 400°C no oxidation is observed. Further heating results in a significant increase of Fe^{3+} and at about 700°C complete oxidation is achieved. In the fully oxidized sample the quadrupole splitting of Fe^{3+} in M3 is notable larger than in the unoxidized sample. The same is probably valid for Fe^{3+} in M1. The stippled lines in the upper part of the figure are drawn to parallel the trend in the Fe^{3+}/Fe_{tot} ratio. Data from Dollase (1973).

samples shows evidence for Fe^{3+} in a site other than M3 or M1, Dollase (1973) concluded that Fe^{2+} in the unoxidized allanite samples is also restricted to M1 and M3. Longer heating at the same temperature did not result in any further oxidation and thus the degree of oxidation is a function of temperature only. Heating an oxidized allanite in a reducing H_2 atmosphere at 680°C for 6.5 hours results in a Mössbauer spectrum identical to that of the untreated sample and indicates that the oxidation process is fully reversible (Dollase 1973). The Mössbauer parameters of the Fe^{3+} doublets in the oxyallanite samples are very consistent (Fig. 20d). Their isomer shifts of 0.353 to 0.36 mm/sec for Fe^{3+} in M3 and 0.335 to 0.355 mm/sec for Fe^{3+} in M1 are comparable to the corresponding ones in the Al-Fe^{3+} solid solutions but their quadrupole splittings of 2.264 to 2.311 mm/sec for Fe^{3+} in M3 and 1.84 to 1.91 mm/sec for Fe^{3+} in M1 are significantly larger than in the Al-Fe^{3+} solid solutions (Figs 20, 23). Unfortunately, Dollase (1973) only provided the Mössbauer parameters for the almost fully oxidized samples ($X_{Fe3+} > 0.88$) but not for the partly oxidized ones. The evolution of the Mössbauer parameters with increasing heating/oxidation can therefore only be assumed (Fig. 23).

Kartashov et al. (2002) reported the Mössbauer spectrum of a ferriallanite with 1.24 Fe^{3+} and 0.93 Fe^{2+} pfu. The spectrum shows three well-resolved doublets (Fig. 19e). Based on their isomer shifts, one of the doublets can be assigned to Fe^{2+} whereas the other two must be assigned to Fe^{3+}. Due to its high Fe content, the Fe must be distributed over all three octahedral sites. The authors therefore assigned the Fe^{2+} doublet (IS = 1.068 mm/sec, OS = 1.62 mm/sec) to Fe^{2+} in M3 and the two Fe^{3+} doublets to Fe^{3+} in M1 and M2, respectively. The Mössbauer parameters of the Fe^{3+} doublets (IS = 0.334 and 0.359 mm/sec and OS = 0.85 and 1.78 mm/sec for Fe^{3+} in M2 and M1, respectively) closely resemble those of the two different low intensity Fe^{3+} doublets in the spectra of the Al-Fe^{3+} solid solutions (see above). It is reasonable to assume that these low intensity Fe^{3+} doublets in the Al-Fe^{3+} solid solutions must therefore be also assigned to M2 and M1, respectively.

Intracrystalline Al-Fe^{3+} partitioning within the Al-Fe^{3+} solid solution series

Dollase (1973), Bird et al. (1988), Patrier et al. (1991), and Fehr and Heuss-Aßbichler (1997) used Mössbauer spectroscopy to study the intracrystalline Al-Fe^{3+} partitioning in Al-Fe^{3+} solid solutions. In good accordance with the structural data, the Mössbauer spectroscopic studies have shown that Fe partitions between the different octahedral sites only for $X_{Ep} > 0.7$ but is confined exclusively to M3 for $X_{Ep} < 0.7$. Consequently, for $X_{Ep} > 0.7$ there will be a non-convergent ordering process of Al and Fe^{3+} between the different octahedral sites whereas for $X_{Ep} < 0.7$ a convergent ordering process occurs (Heuss-Aßbichler 2000).

As discussed above, the Mössbauer parameters provide evidence that Patrier et al. (1991) might have interpreted their recorded spectra incorrectly and these data are therefore neglected in the following discussion. Furthermore, only the Mössbauer spectroscopic data of those samples will be considered, for which P and T of equilibration are known. A detailed discussion and thermodynamic treatment of the non-convergent ordering of Al and Fe^{3+} between the different octahedral sites is given in the chapter on the thermodynamic properties of epidote minerals by Gottschalk (2004; his Figure 20). Dollase (1973) and Fehr and Heuss-Aßbichler (1997) studied the Al–Fe^{3+} partitioning between the M3 and M1 sites in natural, heat treated epidote samples with X_{Ep} = 0.79 to 1.0. Calculating the concentrations of Fe^{3+} in the two sites from the relative areas of the doublets, the data indicate that the amount of Fe^{3+} in M1 increases with increasing total Fe^{3+} content as well as with temperature. For high X_{Ep} values, the relative amount of Fe^{3+} in M1 may reach up to 10 %. Bird et al. (1988) studied natural epidote samples from the Salton Sea geothermal system (see also Bird and Spieler 2004). Based on the probable downhole temperatures, Bird et al. (1988) inferred equilibration temperatures of 260 to 400°C for the studied samples. Some of the estimated Fe^{3+} contents in M1 are notable higher than predicted by the data of Dollase (1973) and Fehr and Heuss-Aßbichler (1997) for these temperatures. Bird et al. (1988) interpreted this higher disorder as a metastable persistence of a former equilibrium stage. Likewise, some of the synthetic samples of Liou (1973) that were studied by Dollase (1973) also show a higher disorder than expected for the synthesis conditions. This probably reflects a metastable higher disorder inherited during the fast growth of the synthetic crystals (Fehr and Heuss-Aßbichler 1997).

Fehr and Heuss-Aßbichler (1997) studied the kinetics of the non-convergent ordering process of Al and Fe^{3+} between M3 and M1. They heat treated two epidote samples with X_{Ep} = 0.79 and 0.98 at 500, 600, and 650°C/0.3 GPa for 1 to 22 days under controlled oxygen fugacities of the hematite/magnetite buffer and determined the Fe^{3+} partitioning between M3 and M1 by means of Mössbauer spectroscopy. The data indicate that already after 5 days equilibrium is achieved. The Mössbauer parameters for Fe^{3+} in M3 and M1, respectively, did not change during the course of the heating experiments and the authors concluded that no change in the bonding character and the local environments of M1 and M3 occurred (Fehr and Heuss-Aßbichler 1997).

The spectra of the Al-Fe^{3+} solid solutions with X_{Ep} = 0.39, 0.43, 0.46, 0.60, and 0.70 studied by Fehr and Heuss-Aßbichler (1997) and Heuss-Aßbichler (2000) are remarkably asymmetric and display an intense peak at high velocity and a broad low velocity peak (Fig. 19a lower two spectra). To account for this asymmetry the authors evaluated the spectra with two only slightly different doublets for ferric Fe besides a very low intensity doublet for Fe^{2+}. The Mössbauer parameters for the two Fe^{3+} doublets are very similar. Their isomer shift is 0.37 to 0.44 and 0.24 to 0.36 mm/sec and their quadrupole splitting is 1.89 to 1.97 and 1.99 to 2.32 mm/sec. In accordance with the general high quadrupole splitting and because Fe^{3+} is exclusively confined to M3 at X_{Ep} < 0.70 (see above), Fehr and Heuss-Aßbichler (1997) and Heuss-Aßbichler (2000) assigned both doublets to a M3 site (labeled M3 and M3´). As the quadrupole splitting of M3´ is slightly higher than that of M3, it must be slightly more distorted. They concluded that in the analyzed samples two epidote phases with slightly different local environments of their respective M3 sites coexist and that at least in the compositional range X_{Ep} = 0.39 to 0.70 immiscibility occurs along the clinozoisite–epidote solid solutions series. This interpretation is consistent with the results of Dollase (1973) who also found asymmetric doublets for Fe^{3+} in M3 in the samples with X_{Ep} = 0.36 and 0.42, but ascribed this unequal broadening of the peaks to relaxation broadening due in part to the long average Fe-Fe distances in the low-Fe clinozoisites.

Because the samples are homogeneous on the microscale according to microprobe analyses and X-ray diffraction data, the immiscibility must form domains in the nanoscale

range (Fehr and Heuss-Aßbichler 1997). Unfortunately, the authors were not able to determine the composition of at least one of the two coexisting phases. By comparison with their results on the intercrystalline exchange of Al–Fe^{3+} between the grossular–andradite and clinozoisite–epidote solid solution series (Heuss-Aßbichler and Fehr 1997) they proposed two solvi in the compositional range X_{Ep} = 0.3 to 0.75 along the clinozoisite–epidote solid solution series that are separated by a small stability field of an intermediate Al-Fe^{3+} solid solution of about X_{Ep} = 0.5.

To test their interpretation with two solvi, Fehr and Heuss-Aßbichler (1997) and Heuss-Aßbichler (2000) heat-treated some of the samples. With increasing temperature, the intensities of the M3 and M3´ doublets changed in accordance with the proposed closure of the solvi and indicate stable phase relations. Stable phase relations were also proven by reversal experiments at different temperatures for one of the studied samples. Although the exact positions of the solvi were not determined, their data strongly suggest that immiscibility occurs along the Al-Fe^{3+} solid solution series (for a structural and thermodynamic treatment of this immiscibility see Franz and Liebscher 2004 and Gottschalk 2004, respectively).

OTHER SPECTROSCOPIC METHODS

Beside the aforementioned spectroscopic methods that were applied to the different epidote minerals by numerous and detailed studies, there are other spectroscopic methods that were only applied by few and singular studies. Therefore these spectroscopic methods will only be shortly reviewed below.

X-ray absorption spectroscopy

X-ray absorption spectroscopy has been applied to Al and Fe^{3+} in natural monoclinic Al-Fe^{3+} solid solutions and to the REE Gd, Er, and Lu in REE rich epidote. Waychunas et al. (1983, 1986) published the first *K*-edge XANES (X-ray absorption near edge structure) and *K*-edge EXAFS (extended X-ray absorption fine structure) powder spectra of Fe^{3+} in epidote of unspecified composition. Later, Waychunas and Brown (1990) recorded polarized single crystal Fe^{3+} *K*-edge XANES and EXAFS spectra of epidote of unspecified composition and Artioli et al. (1995) published the Fe^{3+} *K*-edge XANES powder spectrum of an epidote with X_{Ep} ~1.1. X-ray absorption spectroscopy of Al in epidote minerals is restricted to the Al *K*-edge XANES spectra of two epidotes with X_{Ep} ~0.54 and ~0.79 recorded by Li et al. (1995). The Fe^{3+} *K*-edge XANES powder spectra recorded by Waychunas et al. (1983) and Artioli et al. (1995) reveal three and four main features, respectively. They are characterized by a pre-edge feature at uniform ~7,113 eV and one or two shoulders at ~7,122 eV and ~7,122 and 7,128 eV, respectively. The edge-crest occurs at ~7,129 and ~7,133 eV. The polarized single crystal Fe^{3+} *K*-edge XANES spectra of epidote recorded by Waychunas and Brown (1990) with E parallel [010] and E normal to (100) display the pre-edge feature at 7,112.5 eV (Fig. 24) consistent with the powder spectra. Two shoulders at 7,121.0 and 7,124.0 eV appear only in the E parallel [010] spectrum whereas both spectra show a first large feature at 7,126.0 and 7,126.5 eV, respectively, and a second one at ~7,132 eV (Fig. 24). From the polarized EXAFS spectra Waychunas and Brown (1990) calculated Fe^{3+}–O distances of Fe^{3+}–O2 = 1.952 Å and Fe^{3+}–O1 = 2.225 Å (E parallel [010] spectrum) and mean Fe^{3+}–(O4, O8) = 1.959 Å and Fe^{3+}–O1 = 2.236 Å (E normal (100) spectrum). The unpolarized EXAFS spectrum of Waychunas et al. (1986) gives Fe^{3+}–O1 = 2.253 Å and mean Fe^{3+}–(O2, O4, O8) = 1.954 Å. These results are in fairly good agreement with the XRD data (see Franz and Liebscher 2004).

The Al *K*-edge XANES spectra recorded by Li et al. (1995) yield uniform edge–crest positions of 1,568.0 eV for X_{Ep} ~0.54 and 1,567.8 eV for X_{Ep} ~0.79. Unfortunately, the authors did not publish the spectra nor provide details on further spectral properties.

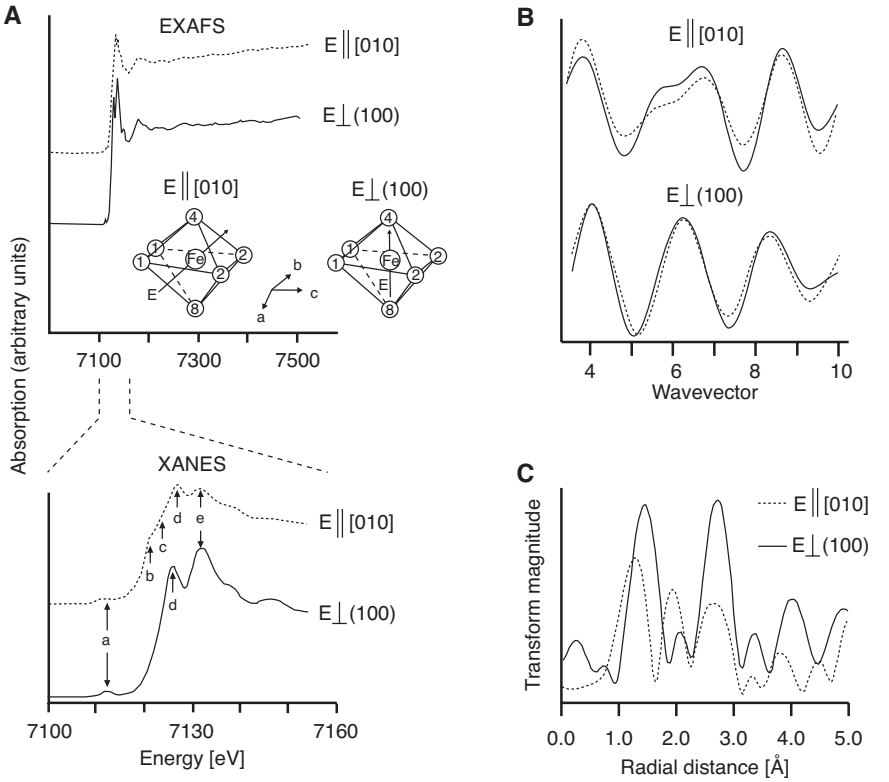

Figure 24. (A) Polarized single crystal XANES and EXAFS spectra of epidote. The polarizations E parallel [010] and E normal to (100) are synonymous with probing the Fe^{3+}–O1, O2 and Fe^{3+}–O4, O8 bonds of the M3 octahedron, respectively (see polyhedra sketches). (B) Epidote polarized EXAFS fitted filtered spectra. Upper part for E parallel [010] and lower part for E normal to (100). Solid lines represent the observed EXAFS, stippled lines the model calculation fit based on two separate Fe–O distances. (C) Polarized EXAFS structure functions of the EXAFS spectra shown in (A). The phase shift functions are not considered and therefore the peaks do not coincide with actual absorber-backscatterer distances. The peak at about 2.0 Å is non-physical and is produced by the large amplitude beat in the EXAFS due to the Fe^{3+}–O1 and Fe^{3+}–O2 distances. Redrawn and modified after Waychunas and Brown (1990).

Cressey and Steel (1988) recorded L_{III} edge EXAFS spectra of Gd, Er, and Lu in synthetic epidote with composition $CaLa_{0.9}X_{0.1}Al_2MgSi_3O_{12}(OH)$ (X = Gd or Er or Lu). Based on detailed multiple shell analysis of EXAFS pair distribution functions and comparing them with those calculated for natural epidote they assigned Gd to the A2 site, Er to A1, and Lu to an octahedral environment, probably M3.

Electron paramagnetic resonance spectroscopy

Electron paramagnetic resonance spectroscopy has been applied to zoisite by Ghose and Tsang (1971), Hutton et al. (1971), and Tsang and Ghose (1971). Ghose and Tsang (1971) and Tsang and Ghose (1971) studied natural V and Mn bearing Al-Fe^{3+} zoisite. Based on the recorded electron paramagnetic resonance spectra they concluded that V is both di- and trivalent and Mn divalent in the studied samples. They assigned Mn^{2+} and Fe^{3+} exclusively to the A1 and M3 sites, respectively. In case of V^{2+} they found evidence that it occupies two

different crystallographic sites and assigned it to the A1 and A2 sites, respectively, with a preference for A1. The electron paramagnetic resonance spectroscopic results of Hutton et al. (1971) on natural untreated and heat-treated zoisite are at variance with those of Ghose and Tsang (1971) and Tsang and Ghose (1971). Hutton et al. (1971) interpreted the line that was attributed to Fe^{3+} by Ghose and Tsang (1971) and Tsang and Ghose (1971) as due to Cr^{3+}. Additionally, Hutton et al. (1971) preclude the existence of V^{2+} but assigned the observed V lines to VO^{2+} and V^{4+} located in M1,2 and M3.

Raman spectroscopy

Le Cleac´h et al. (1988) studied the Raman spectra of zoisite and clinozoisite between 40 and 4,000 cm^{-1}. They observed the lowest optic mode at 115 cm^{-1} in zoisite and at 87 cm^{-1} in clinozoisite. Wang et al. (1994) report the Raman spectrum of an epidote and Huang (1999) the Raman spectrum of a zoisite between 150 and 1,500 cm^{-1} and between 2,800 and 3,800 cm^{-1}. Because Wang et al. (1994) did not provide further details, the band positions can only be estimated. The epidote spectrum is characterized by intense bands at ~400 to 420, ~550, ~910, and ~1080 cm^{-1} and a lack of bands between ~600 and 820 cm^{-1} (Fig. 25). The zoisite spectrum of Huang (1999) displays 19 bands in the range 150 to 1,500 cm^{-1}. Of these bands the most intense one (band 9) occurs at 490 cm^{-1} and is assigned to a Si–O bending mode (Huang 1999). Compared to epidote, the zoisite spectrum is further characterized by band 14 at ~680 cm^{-1}, band 15 at ~870 cm^{-1}, and the bands 18 and 19 at ~1,070 and 1,091 cm^{-1} (Fig. 25). The OH stretching mode in zoisite appears at 3,151 cm^{-1} (Huang 1999).

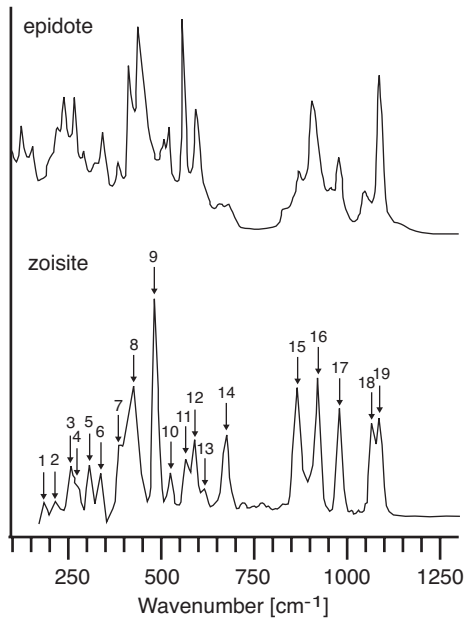

Figure 25. Raman spectra of natural epidote and zoisite of unspecified composition. Redrawn and modified from Wang et al. (1994) and Huang (1999).

Nuclear magnetic resonance spectroscopy

Nuclear magnetic resonance (NMR) spectroscopy on epidote minerals is restricted to the studies by Brinkmann et al. (1969) and Alemany et al. (2000) on zoisite. Brinkmann et al. (1969) studied the nuclear magnetic resonance of ^{27}Al and ^{1}H in zoisite. For Al in M1,2 and M3 they found quadrupole coupling constants (e^2qQ/h) and asymmetry parameters (η) of e^2qQ/h = 8.05 ± 0.12 MHz and η = 0.46 ± 0.01 for M1,2 and e^2qQ/h = 18.50 ± 0.05 MHz and η = 0.160 ± 0.005 for M3. The nuclear magnetic resonance of ^{1}H confirms the proton position as deduced from X-ray diffraction data (Brinkmann et al. 1969). Alemany et al. (2000) studied the nuclear magnetic resonance of ^{27}Al in zoisite by single-puls magic-angle spinning (MAS), selective Hahn echo MAS, and 3QMAS NMR spectroscopy and determined the isotropic chemical shift (δ_{CS}), e^2qQ/h, and η for Al in M1,2 and M3. With e^2qQ/h = 7.9 ± 0.1 MHz and η = 0.51 ± 0.05 for M1,2 and e^2qQ/h = 18.4 ± 0.1 MHz and η = 0.16 ± 0.01 for M3 their data agree well with those of Brinkmann et al. (1969). The isotropic chemical shift is δ_{CS} = 10.7 ± 0.2 ppm for M1,2 and δ_{CS} = 8.0 ± 0.2 ppm for M3. From their data Alemany et al. (2000) conclude that the signal of the distorted M3 site can be observed in MAS NMR spectra that were obtained with

fields of at least 11.7 T and spinning speeds over 30 kHz. The signal intensity of the distorted M3 site is increased significantly in MQMAS NMR experiments using amplitude-modulated pulses to generate double frequency sweeps.

CONCLUDING REMARKS

The numerous spectroscopic studies applied to the epidote minerals have established a profound knowledge of the crystal chemical characteristics of these minerals. Optical absorption and Mössbauer spectroscopy elucidate the valence states and site preferences of the transition metal ions in epidote minerals. Infrared spectroscopy has been proven a powerful tool to study structural changes within the different solid solution series and to distinguish between orthorhombic and monoclinic epidote minerals as well as to determine the respective compositions. However, there are still some open questions. Within the well-established framework, promising and also challenging topics for future spectroscopic work include:

(i) Only few studies recorded pressure dependent optical absorption spectra and their results are inconsistent. More studies on this topic will help to solve this inconsistency and also to derive precise compression moduli for individual octahedral.

(ii) X-ray data indicate that Fe^{3+} also substitute in M2 in monoclinic Al-Fe^{3+} solid solutions. Mössbauer studies have so far assigned all Fe^{3+} doublets in monoclinic Al-Fe^{3+} solid solutions to either M3 or M1. As recommended in this review, one kind of doublet may be assigned to M2. Future Mössbauer studies should try to verify or falsify this recommendation. Best suited for this purpose are synthetic monoclinic Al-Fe^{3+} solid solutions for which precise X-ray data indicate Fe^{3+} in M3, M1, and also M2.

(iii) The intracrystalline ordering of Fe^{3+} in monoclinic Al-Fe^{3+} solid solutions can be studied by Mössbauer spectroscopy. Unfortunately, the exact positions and closure temperatures of the proposed solvi are still not known. To unravel the question of immiscibility along the clinozoisite–epidote solid solution join is probably one of the most important and promising topics for future studies.

(iv) Natural zoisite and clinozoisite samples often show very fine lamellae that are too fine to be resolved by electron microprobe. The different interference colors of these lamellae suggest them to represent coexisting zoisite and clinozoisite. Infrared spectroscopic studies on such specimens would help to distinguish between zoisite and clinozoisite and to determine the composition of both.

(v) Mössbauer spectra of zoisite are completely lacking. As the iron content in natural zoisite is generally low, Mössbauer spectra of zoisite should be recorded on synthetic zoisite doped with ^{57}Fe.

ACKNOWLEDGMENTS

This review benefited from thorough and critical readings by M. Koch-Müller and M. Andrut. Fruitful discussions during the preparation of the manuscript with M. Koch-Müller, I. Abs-Wurmbach, and M. Wilke are gratefully acknowledged. Prof. Jan Stanek from Kraków kindly provided some literature. Throughout the preparation of the manuscript, K. Mai and S. Bernau helped with literature search, figure drawing, and proof reading.

REFERENCES

Abu-Eid (1974) Absorption spectra of transition metal-bearing minerals at high pressures. *In*: The Physics and Chemistry of Minerals and Rocks. Strens RGJ (ed) Wiley, New York, p 641-675

Alemany LB, Callender RL, Barron AR, Steuernagel S, Iuga D, Kentgens APM (2000) Single-pulse MAS, selective Hahn echo MAS, and 3QMAS NMR Studies of the mineral zoisite at 400, 500, 600, and 800 MHz. Exploring the limits of Al NMR detectability. J Phys Chem B 104:11612-11616

Artioli G, Quartieri S, Deriu A (1995) Spectroscopic data on coexisting prehnite-pumpellyite and epidote-pumpellyite. Can Mineral 33:67-75

Bancroft GM, Maddock AG, Burns RG (1967) Applications of the Mössbauer effect to silicate mineralogy. I. Iron silicates of known crystal structure. Geochim Cosmochim Acta 31:2219-2246

Bellamy LJ, Owen AJ (1969) A simple relationship between the infrared stretching frequencies and the hydrogen bond distance in crystals. Spectrochim Acta 25A:329-333

Belov NV, Rumanova JM (1954) The crystal structure of epidote. Trudy Inst Krist Akad Nauk SSSR 9:103-164 (Abstract in Struct Rep 18:544-545)

Bird D, Spieler AR (2004) Epidote in geothermal systems. Rev Mineral Geochem 56:235-300

Bird DK, Cho M, Janik CJ, Liou JG, Caruso LJ (1988) Compositional, order/disorder, and stable isotope characteristics of Al-Fe epidote, state 2-14 drill hole, Salton Sea Geothermal System. J Geophys Res 93: 13135-13144

Bonazzi P, Menchetti S (2004) Manganese in monoclinic members of the epidote group: piemontite and related minerals. Rev Mineral Geochem 56:495-552

Bonazzi P, Menchetti S, Palenzona A (1990) Strontiopiemontite, a new member of the epidote group, from Val Graveglia, Liguria, Italy. Eur J Mineral 4:519-523

Bradbury SE, Williams Q (2003) Contrasting bonding behavior of two hydroxyl-bearing metamorphic minerals under pressure: Clinozoisite and topaz. Am Mineral 88:1460-1470

Brinkmann D, Staehli JL, Ghose S (1969) Nuclear magnetic resonance of ^{27}Al and ^{1}H in zoisite, $Ca_2Al_3Si_3O_{12}(OH)$. J Chem Phys 51:5128-5133

Brunsmann A (2000) Strukturelle, kristallchemische und phasenpetrologische Untersuchungen an synthetischen und natürlichen Zoisit und Klinozoisit Mischkristallen. Dissertation, Technical University of Berlin, Germany (*http://edocs.tu-berlin.de/diss/2000/brunsmann_axel.htm*)

Burns RG, Strens RGJ (1967) Structural interpretation of polarized absorption spectra of the Al-Fe-Mn-Cr epidotes. Min Mag 36:204-226

Catti M, Ferraris G, Ivaldi G (1989) On the crystal chemistry of strontian piemontite with some remarks on the nomenclature of the epidote group. N Jahrb Mineral Monatsh 1989:357-366

Cech F, Vrána S, Povondra P (1972) A non-metamict allanite from Zambia. N Jahrb Miner Abh 116:208-223

Comodi P, Zanazzi PF (1997) The pressure behavior of clinozoisite and zoisite: An X-ray diffraction study. Am Mineral 82:61-68

Cressey G, Steel AT (1988) An EXAFS study of Gd, Er, and Lu site location in the epidote structure. Phys Chem Mineral 15:304-312

Cynn H, Hofmeister A (1994) High-pressure IR spectra of lattice modes and OH vibrations in Fe-bearing wadsleyite. J Geophys Research B 99:717-727

De Coster M, Pollak H, Amelinckx S (1963) A study of Mössbauer absorption in iron silicates. Physica Stat Solidi 3:283-288

Della Ventura G, Mottana A, Parodi GC, Griffin WL (1996) FTIR spectroscopy in the OH-stretching region of monoclinic epidotes from Praborna (St. Marcel, Aosta Valley, Italy). Eur J Mineral 8:655-665

Dollase WA (1968) Refinement and comparison of the structures of zoisite and clinozoisite. Am Mineral 53: 1882-1898

Dollase WA (1969) Crystal structure and cation ordering of piemontite. Am Mineral 54:710-717

Dollase WA (1971) Refinement of the crystal structures of epidote, allanite and hancockite. Am Mineral 56: 447-464

DollaseWA (1973) Mössbauer spectra and iron distribution in the epidote group minerals. Z Kristallogr 138: 41-63

Farmer VC (1974) Orthosilicates, pyrosilicates, and other finite-chain silicates. *In:* The Infrared Spectra of Minerals 4. Monograph of the Mineralogical Society. Farmer VC (ed) Mineralogical Society, London, p 285-303

Faye GH, Harris DC (1969) On the origin of colour and pleochroism in andalusite from Brazil. Can Mineral 10:47-56

Faye GH, Nickel EH (1971) On the pleochroism of vanadium-bearing zoisite from Tanzania. Can Mineral 10: 812-821

Fehr KT, Heuss-Aßbichler S (1997) Intracrystalline equilibria and immiscibility along the join clinozoisite–epidote: An experimental and ^{57}Fe Mössbauer study. N Jahrb Mineral Abh 172:43-76

Ferraris G, Ivaldi G, Fuess H, Gregson D (1989) Manganese/iron distribution in a strontian piemontite by neutron diffraction. Z Krist 187:145-151

Franz G, Liebscher A (2004) Physical and chemical properties of the epidote minerals–an introduction. Rev Mineral Geochem 56:1-82

Gavorkyan SV (1990) IR spectra of epidote-group minerals. Mineralogiceskij zurnal 12:63-66 (in Russian)

Ghose S, Tsang T (1971) Ordering of V^{2+}, Mn^{2+}, and Fe^{3+}-ions in zoisite, $Ca_2Al_3Si_3O_{12}$ (OH). Science 171: 374-376

Gieré R, Sorensen SS (2004) Allanite and other REE-rich epidote-group minerals. Rev Mineral Geochem 56: 431-494

Giuli G, Bonazzi P, Menchetti S (1999) Al-Fe disorder in synthetic epidotes: a single-crystal X-ray diffraction study. Am Mineral 84: 933-936

Gottschalk M (2004) Thermodynamic properties of zoisite, clinozoisite and epidote. Rev Mineral Geochem. 56:83-124

Grodzicki M, Heuss-Aßbichler S, Amthauer G (2001) Mössbauer investigations and molecular orbital calculations on epidote. Phys Chem Mineral 28:675-681

Grum-Grzhimailo SV, Brilliantov NA, Sviridov DT, Sviridova RK, Sukhanova ON (1963) Absorption spectra of crystals containing Fe^{3+} at temperatures down to 1.7 K. Opt Spect 14:118-120 (in Russian)

Hanisch K, Zemann J (1966) Messung des Ultrarot-Pleochroismus von Mineralen. IV. Der Pleochroismus der OH-Streckfrequenz in Epidot. N Jahrb Miner Monatsh:19-23

Herzberg G (1950) Molecular Spectra and Molecular Structure. Van Nostrand, New York

Heuss-Aßbichler S (2000) Ein neues Ordnungsmodell für die Mischkristallreihe Klinozoisit-Epidot und das Granat-Epidot-Geothermometer. Habilitationthesis, München, 105 pp

Heuss-Aßbichler S, Fehr KT (1997) Intercrystalline exchange of Al and Fe^{3+} between grossular-andradite and clinozoisite-epidote solid solutions. N Jahrb Mineral Abh 172:69-100

Holland TJB, Redfern SAT, Pawley AR (1996) Volume behavior of hydrous minerals at high pressure and temperature: II. Compressibilities of lawsonite, zoisite, clinozoisite, and epidote. Am Mineral 81:341-348

Huang E (1999) Raman spectroscopic study of 15 gem minerals. J Geol Soc China 42:301-318

Hutton DR, Troup GJ, Stewart GA (1971) Paramagnetic ions in zoisite. Science 174:1259

Ito T, Morimoto N, Sadanga R (1954) On the structure of Epidote. Acta Crystallographica 7:53-59

Janeczek J, Sachanbinski M (1989) Chemistry and zoning of thulite from the Wiry magnesite deposit, Poland. N Jahrb Miner Monatsh:325-333

Kartashov PM, Ferraris G, Ivaldi G, Sokolova E, McCammon CA (2002) Ferriallanite-(Ce), $CaCeFe^{3+}AlFe^{3+}(SiO_4)(Si_2O_7)O(OH)$, a new member of the epidote group: Description, X-ray and Mössbauer study. Can Mineral 40:1641-1648

Kersten M, Langer K, Almen H, Tillmanns E (1988) The polarized single crystal spectra and structures of synthetic thulite and piemontites, $Ca_2Al_{3-p}Mn^{3+}_p[O/OH/SiO_4/Si_2O_7]$, with $0.5 \le p \le 1.6$. Z Kristall 185: 111

Kiseleva IA, Ogorodnikova LP (1987) Calorimetric data on the thermodynamics of epidote, clinozoisite, and zoisite. Geochem Int 24:91-98

Langer K (1990) High pressure spectroscopy. *In*: Absorption Spectroscopy in Mineralogy. Mottana A, Burragato F (eds) Elsevier, Amsterdam, p 228-284

Langer K, Abu-Eid RM (1977) Measurements of the polarized absorption spectra of synthetic transition metal-bearing silicate microcrystals in the spectral range 44,000-4,000 cm^{-1}. Phys Chem Mineral 1:273-299

Langer K, Lattard D (1980) Identification of a low-energy OH-valence vibration in zoisite. Am Mineral 65: 779-783

Langer K, Raith M (1974) Infrared spectra of Al-Fe(III)-epidotes and zoisites, $Ca_2(Al_{1-p}Fe^{3+}_p)Al_2O(OH)[Si_2O_7][SiO_4]$. Am Mineral 59:1249-1258

Langer K, Abu-Eid RM, Anastasiou P (1976) Absorptionsspektren synthetischer Piemontite in den Bereichen 43000-11000 cm^{-1} (232,6-909,1 nm) und 4000-250 cm^{-1} (2,5-40 μm). Z Kristall 144:434-436

Langer K, Tillmanns E, Kersten M, Almen H, Arni RK (2002) The crystal chemistry of Mn^{3+} in the clino- and orthozoisite structure types, $Ca_2M^{3+}_3[OH/O/SiO_4/Si_2O_7]$: A structural and spectroscopic study of some natural piemontites and "thulites" and their synthetic equivalents. Z Kristall 217:563-580

Lazarev AN (1972) Vibrational Spectra and Structure of Silicates. Plenum, New York.

Le Cleac'h A, Gillet P, Putnis A (1988) IR, Raman spectra and thermodynamic properties of zoisite and clinozoisite. Terra Cognita 8:70

Li D, Bancroft GM, Fleet ME, Feng XH, Pan Y (1995) Al *K*-edge XANES spectra of aluminosilicate minerals. Am Mineral 80:432-440

Liebscher A, Gottschalk M (2004) The *T-X* dependence of the isosymmetric displacive phase transition in synthetic Fe^{3+}-Al zoisite: A temperature-dependent infrared spectroscopy study. Am Mineral 89:31-38

Liebscher A, Gottschalk M, Franz G (2002) The substitution Fe^{3+}-Al and the isosymmetric displacive phase transition in synthetic zoisite: A powder X-ray and infrared spectroscopy study. Am Mineral 87:909-921

Linke W (1970) Messung des Ultrarot-Pleochroismus von Mineralen. X. Der Pleochroismus der OH-Streckfrequenz in Zoisit. Tschermaks Mineral Petrogr Mitt 14:61-63

Liou JG (1973) Synthesis and stability relations of epidote, $Ca_2Al_2FeSi_3O_{12}(OH)$. J Petrol 14:381-314

Lipka J, Petrik I, Tóth I, Gajdosová M (1995) Mössbauer study of allanite. Acta Phys Slovaca 45:61-66

Marfunin AS, Mineyeva RM, Mkrtchyan AR, Nyussik YM, Fedorov VY (1967) Optical and Mössbauer spectroscopy of iron in rock-forming silicates. Seriya Geologicheskaya 10:86-102 (in Russian)

Mingsheng P, Daoyuan R (1986) A spectroscopic study on the allanite from a granite body in northeastern Guangdong. J Central-South Inst Mining Metall 4:1-9 (in Chinese)

Mingsheng P, Dien L (1987) Spectroscopy, genesis, and process properties of partly metamict allanite. J Central-South Inst Mining Metall 18:362-368

Moenke H (1962) Mineral-Spektren. Akademie Verlag Berlin

Paesano A, Kunrath JI, Vasquez A (1983) A ^{57}Fe Mössbauer study of epidote. Hyperfine Interactions 15/16: 841-844

Parkin KM, Burns RG (1980) High temperature crystal field spectra of transition metal-bearing minerals: Relevance to remote-sensed spectra of planetary surfaces. Proc 11th Lunar Planet Sci Conf 1:731-755

Patrier P, Beaufort D, Meunier A, Eymery JP, Petit S (1991) Determination of the nonequilibrium ordering state in epidote from the ancient geothermal field of Saint Martin: Application of Mössbauer spectroscopy. Am Mineral 76:602-610

Pawley AR, Redfern SAT, Holland TJB (1996) Volume behavior of hydrous minerals at high pressure and temperature: I. Thermal expansion of lawsonite, zoisite, clinozoisite, and diaspore. Am Mineral 81:335-340

Perseil EA (1987) Particularités des piémontites de Saint-Marcel-Praborna (Italie); spectres IR. Actes du 112. Congrès National des Sociétés Savantes. Edition du CTHS, Paris.

Petrusenko S, Taran MN, Platonov AN Gavorkyan SV (1992) Optical and infrared spectoscopic studies of epidote group minerals from the Rhodope region. Rev Bulgarian Geol Soc 53:1-9 (in Russian)

Pollack H, Bruyneel W (1975) On the iron distribution between sites in epidote. *In*: Hrynkiewicz AZ, Sawicki JA (eds) Proceedings of the international Conference on Mössbauer Spectroscopy, Cracow, Poland, 259-260

Robinson K, Gibbs GV, Ribbe PH (1971) Quadratic elongation: A quantitative measure of distortion in coordination polyhedra. Science 172:567-570

Salje EKH, Carpenter MA, Malcherek T, Boffa Ballaran T (2000) Autocorrelation analysis of infrared spectra from minerals. Eur J Mineral 12:503-519

Schmetzer K, Bank H (1979) Bluish-green zoisite from Merelani, Tanzania. J Gemm 16:512-513

Schmetzer K, Berdesinski W (1978) Das Absorptionsspektrum von Cr^{3+} in Zoisit. N Jb Mineral Monatsh: 197-202

Scott H, Williams Q (1999) An infrared spectroscopic study of lawsonite to 20 GPa. Phys Chem Mineral 26: 437-445

Smith G, Hålenius U, Langer K (1982) Low temperature spectral studies of Mn^{3+}-bearing andalusite and epidote type minerals in the range 30,000-5,000 cm^{-1}. Phys Chem Mineral 8:136-142

Smith JV, Pluth JJ, Richardson Jr JW, Kvick A (1987) Neutron diffraction study of zoisite at 15 K and X-ray study at room temperature. Z Kristall 179:305-321

Taran MN, Langer K (2000) Electronic absorption spectra of Fe^{3+} in andradite and epidote at different temperatures and pressures. Eur J Mineral 12:7-15

Taran MN, Platonov AN, Petrusenko SI, Khomenko VM, Belichenko VP (1984) Optical absorption spectra of Mn^{3+} ion in natural clinozoisites. Geochem Mineral Petrol 19:43-51 (in Russian)

Tsang T, Ghose S (1971) Electron paramagnetic resonance of V^{2+}, Mn^{2+}, Fe^{3+} and optical spectra of V^{3+} in blue zoisite, $Ca_2Al_3Si_3O_{12}(OH)$. J Chem Phys 4,3:856-862

Wang A, Han J, Guo L, Yu J, Zeng P (1994) Database of standard Raman spectra of minerals and related inorganic crystals. Applied Spectroscopy 48:959-968

Waychunas GA, Brown Jr GE (1990) Polarized X-ray absorption spectroscopy of metal ions in minerals. Phys Chem Mineral 17:420-430

Waychunas GA, Apted MJ. Brown Jr GE (1983) X-ray K-edge absorption spectra of Fe minerals and model compounds: Near-edge structure. Phys Chem Mineral 10:1-9

Waychunas GA, Brown Jr GE, Apted MJ (1986) X-ray K-edge absorption spectra of Fe minerals and model compounds: II. EXAFS. Phys Chem Mineral 13:31-47

White WB, Keester KL (1966) Optical absorption spectra of iron in the rock-forming silicates. Am Mineral 51:774-791

Williams Q (1992) A vibrational spectroscopic study of hydrogen in high-pressure mineral assemblages. *In*: High-Pressure Research: Application to Earth and Planetary Sciences. Syono Y, Manghnani MH (eds) Am Geopyhs Union, Washington D.C., p 289-296

Winkler B, Langer K, Johannsen PG (1989) The influence of pressure on the OH-valence vibration of zoisite. Phys Chem Mineral 16:668-671

Wood BJ, Strens RGJ (1972) Calculation of crystal field splittings in distorted coordination polyhedra: spectra and thermodynamic properties of minerals. Mineral Mag 38:909-917